AFCEC-TR-76-4

EVALUATION OF SUBSTITUTE INPUT FOR NCEL BOMB DAMAGE REPAIR CODE

ERIC H. WANG CIVIL ENGINEERING RESEARCH FACILITY
UNIVERSITY OF NEW MEXICO
UNIVERSITY HILL, CAMPUS POST OFFICE
ALBUQUERQUE, NEW MEXICO 87131

MARCH 1976

FINAL REPORT: JANUARY 1975 - OCTOBER 1975

AIR FORCE CIVIL ENGINEERING CENTER
(AIR FORCE SYSTEMS COMMAND)
TYNDALL AIR FORCE BASE
FLORIDA 32401

UNCLASSIFIED

SECURITY CLASSIFICATION OF THIS PAGE (When Data Entered)

REPORT DOCUMENTATION PAGE

READ INSTRUCTIONS BEFORE COMPLETING FORM

1. REPORT NUMBER: AFCEC TR-76-4	2. GOVT ACCESSION NO.
3. RECIPIENT'S CATALOG NUMBER	
4. TITLE (and Subtitle): EVALUATION OF SUBSTITUTE INPUT FOR NCEL BOMB DAMAGE REPAIR CODE	5. TYPE OF REPORT & PERIOD COVERED: Final rept. 6 Jan [illegible] - 6 Oct [illegible]75
	6. PERFORMING ORG. REPORT NUMBER: CERF-AP-16
7. AUTHOR(s): Glenn T. Baird	8. CONTRACT OR GRANT NUMBER(s): F29601-74-C-0030 I.D. 5.10/01
9. PERFORMING ORGANIZATION NAME AND ADDRESS: Eric H. Wang Civil Engineering Research Facility, University of New Mexico, University Hill, Campus Post Office, Albuquerque, NM 87131	10. PROGRAM ELEMENT, PROJECT, TASK AREA & WORK UNIT NUMBERS: AF-2164 21044B
11. CONTROLLING OFFICE NAME AND ADDRESS: Air Force Civil Engineering Center, Air Force Systems Command, Tyndall Air Force Base, FL 32401	12. REPORT DATE: March [illegible]976
	13. NUMBER OF PAGES: 58
14. MONITORING AGENCY NAME & ADDRESS (if different from Controlling Office)	15. SECURITY CLASS (of this report): Unclassified
	15a. DECLASSIFICATION/DOWNGRADING SCHEDULE: --

16. DISTRIBUTION STATEMENT (of this Report)

Approved for public release; distribution unlimited.

17. DISTRIBUTION STATEMENT (of the abstract entered in Block 20, if different from Report)

18. SUPPLEMENTARY NOTES

Available in DDC

19. KEY WORDS (Continue on reverse side if necessary and identify by block number)

Finite Element
Bomb Damage Repair
Soil Mechanics
Bulk Modulus
Shear Modulus
Modulus of Elasticity

20. ABSTRACT (Continue on reverse side if necessary and identify by block number)

This research project was concerned with the evaluation of substitute input to a computer program which is used to analyze the performance of repaired bomb craters. The typical materials used in the rapid repair of bomb craters were tested in various states of stress to obtain soil strength and deformation parameters for use in the computer code. A concrete sand, two gravels, and a well-graded crushed limestone were tested in hydrostatic compression, constant mean normal stress, and triaxial compression for evaluation of their nonlinear bulk moduli, shear moduli, and moduli of elasticity. Laboratory testing was performed with

DD FORM 1473 EDITION OF 1 NOV 65 IS OBSOLETE (over) SN 0102-014-6601

Block No. 20 (Continued) (cf p 1473A)

a modified Hveem Stabilometer, modified as a triaxial compression apparatus. Bulk and shear moduli were inputted to the axisymmetric, finite-element computer code and the nonlinear results were compared with the linear results. Triaxial compression confining pressures are suggested for the selected materials. With the linear moduli computed from the triaxial compression tests performed at these pressures, deflections equivalent to those computed with nonlinear moduli can be computed. The computer input was thereby reduced and laboratory testing was greatly simplified.

PREFACE

This report was prepared by the University of New Mexico Civil Engineering Research Facility (UNM-CERF), Albuquerque, New Mexico and was funded under Contract Number F29601-74-C-0030 with the Air Force Civil Engineering Center, Tyndall Air Force Base, Florida. The project was initiated by the Air Force Weapons Laboratory, Kirtland Air Force Base, New Mexico, and then transferred to AFCEC.

Work was performed at the CERF facilities by the Soil Mechanics and Pavements Division under the supervision of Division Manager John P. Nielsen, who also reviewed the report prior to publication. The author gratefully acknowledges the technical support given by Vincent Cassino, Soil Mechanics and Pavements Division, CERF, who conducted the laboratory testing, and William Moore of CERF, Theoretical Division, for assistance in operating the BDR Code.

Additional insight and direction of the project were supplied by Project Officer Lt. Raymond S. Rollings, AFCEC, and Capt. Lawrence D. Hokanson, AFIT, Wright-Patterson Air Force Base, Ohio. Consultations and advice given by John Crawford of the Civil Engineering Laboratory, Port Hueneme, California, greatly aided the operation of the NCEL BDR Code and selection of the code input parameters.

This report has been reviewed by the Information Officer (IO) and is releasable to the National Technical Information Service (NTIS). At NTIS, it will be available to the general public, including foreign nations.

This technical report has been reviewed and is approved for publication.

RAYMOND S. ROLLINGS, 1st Lt, USAF
Project Officer

GUY P. YORK, Lt Col, USAF
Director of Engineering Materials

ROBERT E. BRANDON
Technical Director

ROBERT M. ITEN, Colonel, USAF
Commander

TABLE OF CONTENTS

Section	Title	Page
I	INTRODUCTION	5
II	STRESS/STRAIN RELATIONSHIPS	7
III	TEST METHODS	10
	Introduction	10
	Hydrostatic Compression Test	10
	Constant Mean Normal Stress Test	10
	Triaxial Test	15
	Summary	17
IV	LABORATORY TESTING	18
	Materials	18
	Samples	18
	Equipment and Setup	20
	Test Results	22
V	COMPUTER ANALYSIS	31
	Computer Code	31
	Crater Model	32
	Analytical Procedure	33
	Computed Results	36
	Nonlinear Analysis	36
	Linear Analysis	42
	Comparison of Nonlinear and Linear Data	45
VI	CONCLUSIONS AND RECOMMENDATIONS	52
	REFERENCES	54
	ABBREVIATIONS, ACRONYMS, AND SYMBOLS	55

LIST OF ILLUSTRATIONS

Figure	Title	Page
1	Stress Components	8
2	Hydrostatic Compression Test Method	11
3	Constant Mean Normal Stress Test Method	13
4	Standard Triaxial Compression Test Method	16
5	Gradation Curves for Fill Materials	19
6	Frozen Sample in Standard Proctor Compaction Mold	21
7	Frozen Sample of 3/4-Inch-Diameter Gravel	21
8	Hveem Stabilometer and CERF-Designed Equipment	23
9	Stabilometer Test Setup	23
10	Hydrostatic Compression Test Data	24
11	Moisture/Density Curve for Crushed Limestone	25
12	Hydrostatic Compression Test Data for Crushed Limestone at Various Densities	26
13	NCEL Gradation Curve for Sand	27
14	Hydrostatic Compression Test Data for Sand in Loose and Dense States	27
15	Constant Mean Normal Stress Test Data	29
16	Standard Triaxial Compression Test Data	30
17	Finite-Element Mesh with Crater Profiles	34
18	Detailed Model of Crater	35
19	Deflection Basins for 12-Inch-Thick Fill Materials	38
20	Nonlinear Behavior of Backfill Systems	39
21	Vertical Stress Profiles for 12-Inch-Thick Fill Materials	40
22	Vertical Stress Profiles for Crushed Limestone (Second Analysis)	41
23	Effect of Compacted Pushback Material Properties on Deflection	43
24	Effect of Crater Material Properties on Deflection	44
25	Effect of Poisson's Ratio on Deflection	46
26	Effect of Fill Material Thickness on Deflection	47
27	Comparison of Nonlinear and Linear Analyses of Fill Materials	48

LIST OF TABLES

Table	Title	Page
1	NCEL Test Results on Sand.	28
2	Material Characteristics for Silty Clay from Kansas Craters	33
3	Computed Deflections from Nonlinear Data	37
4	Suggested Triaxial Compression Test Confining Pressures.	51

SECTION I
INTRODUCTION

BACKGROUND

In many parts of the world the outcome of military conflicts is dependent upon the ability of base personnel to maintain runways, taxiways, and aprons in an operational condition for attack aircraft. In the case of enemy bombing, this requires rapid and efficient repair of bomb-damaged pavements. The Air Force has been concerned with this problem since 1951 and has sponsored projects directed toward damage prediction (i.e., expected size of bomb craters). Air Force interest now lies in rapid repair methods and performance evaluation of repaired bomb craters. With respect to crater performance, a computer code, which can predict the response of a repaired crater to aircraft loads, has been developed. This code, the NCEL Bomb Damage Repair (BDR) Code, calculates the stresses, strains, and deflections of a repaired crater using the bulk and shear moduli of the backfill materials. However, these moduli are determined by sophisticated laboratory tests, and if the BDR Code is to be used as an operational tool for the prediction of repaired crater performance, simpler material test methods need to be developed.

OBJECTIVE

The objective of this project was to suggest and evaluate soil-testing procedures which could be used to obtain material stress/strain characteristics for use in the BDR Code. These procedures should require only semi-skilled technicians and equipment which can be used routinely in the field or laboratory.

SCOPE

Soil mechanics literature was reviewed for possible substitute test methods which would produce data from which bulk and shear moduli could be calculated.

his approach was necessary because no alterations of the BDR Code were authorized. Although it would be a simple matter to modify the code to use linear soil properties, the resulting computer predictions would not be valid since bomb craters must be repaired rapidly and rapid repair techniques do not allow sufficient soil compaction; thus, the materials most certainly would behave in a nonlinear manner. Therefore, a simple triaxial type test was used to estimate the elastic moduli of the repair materials and these were then used to calculate the required bulk and shear moduli values. The soil properties obtained in this manner were inputted to the BDR Code and the effect of their variation was studied on the code output. The accuracy of this substitute input was determined by comparing it with the nonlinear bulk and shear moduli.

This approach was necessary because no alterations of the BDR Code were authorized. Although it would be a simple matter to modify the code to use linear soil properties, the resulting computer predictions would not be valid since bomb craters must be repaired rapidly and rapid repair techniques do not allow sufficient soil compaction; thus, the materials most certainly would behave in a nonlinear manner. Therefore, a simple triaxial type test was used to estimate the elastic moduli of the repair materials and these were then used to calculate the required bulk and shear moduli values. The soil properties obtained in this manner were inputted to the BDR Code and the effect of their variation was studied on the code output. The accuracy of this substitute input was determined by comparing it with the nonlinear bulk and shear moduli.

SECTION II
STRESS/STRAIN RELATIONSHIPS

The BDR Code uses the bulk modulus and the shear modulus to model a material's response to a stress. A general state-of-stress can be separated into volumetric components and deviatoric components (Figure 1) according to elastic theory (References 1, 2, and 3). Each of these components, which can be determined by tests unique to the modulus, is particularly applicable to soils. The bulk and shear moduli are evaluated by performing a hydrostatic compression test and a constant mean normal stress test, respectively, on the soil.

The modulus of elasticity, E, relates the normal stress, σ, to the resulting normal strain, ε. Normal strain is defined by the change in length of the material divided by its original length.

$$\varepsilon = \Delta\ell/\ell_0$$

$$E = \sigma/\varepsilon$$

For a three-dimensional object, three normal strains are possible, ε_1, ε_2, and ε_3, corresponding to the three orthogonal axes. Poisson's ratio, μ, defines the relationships between ε_1, ε_2, and ε_3.

The bulk modulus, K, relates the hydrostatic, isotropic stress, σ_h, on a material to the volumetric strain, ε_v, it produces. Volumetric strain, ε_v, is the sum of the principal strains, ε_1, ε_2, and ε_3.

$$\varepsilon_v = \varepsilon_1 + \varepsilon_2 + \varepsilon_3$$

---

1. Domashuk, Leonard, Wade, Neil H., "A Study of the Bulk and Shear Moduli of Sand," *J. Soil Mech.a.Found. Div.*, ASCE, March 1969, pp. 561-581.

2. Timoshenko, S., *Theory of Elasticity*, McGraw-Hill, New York and London, 1934.

3. Desai, Chandrakant S., Abel, John F., *Introduction to the Finite Element Method*, Van Nastrand Reinhold Co., New York, 1972.

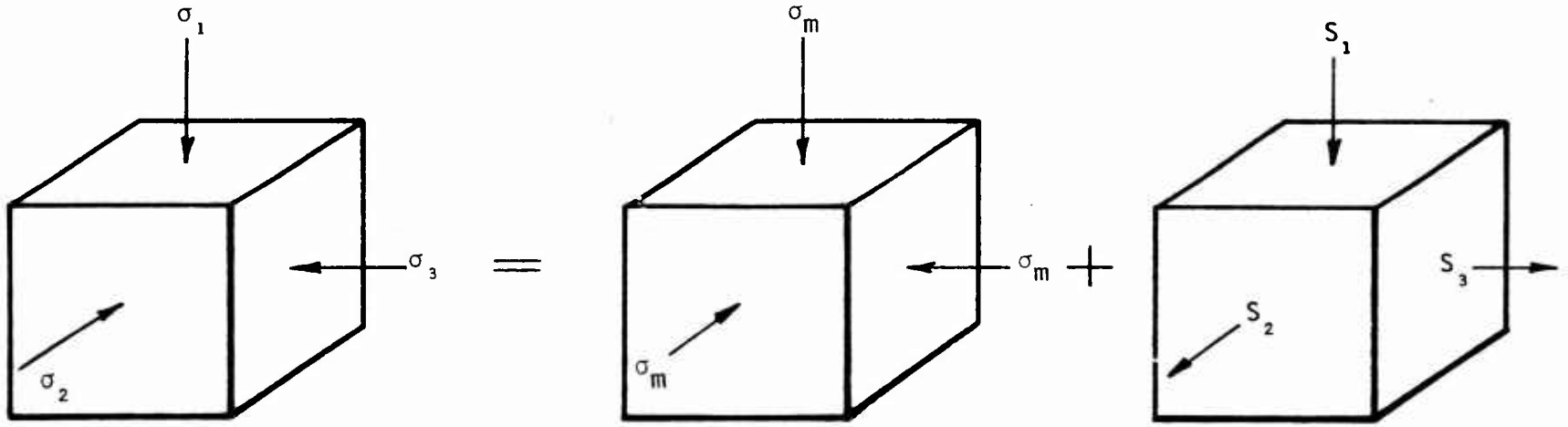

(a) General State-of-Stress

(b) Mean Normal Stress Components

(c) Deviatoric Components

[after Domashuk (Reference 1)]

Figure 1. Stress Components

$$K = \sigma_h/\varepsilon_v$$

The shear modulus, G, relates the shearing stress, τ, to the shearing strain, γ.

$$G = \tau/\gamma$$

The three moduli are interrelated in the following equations:

$$K = \frac{E}{3(1 - 2\mu)}$$

and

$$G = \frac{E}{2(1 + \mu)}$$

SECTION III
TEST METHODS

INTRODUCTION

The nonlinear behavior of the crater backfill and in-situ soils must be known in order to implement the NCEL BDR Code. Nonlinear bulk and shear moduli, expressed as a function of volumetric strain, are used in the code. Three types of tests are employed to determine the nonlinear properties of the materials. Hydrostatic compression tests describe the variation in bulk modulus; a series of constant mean normal stress tests determines the shear behavior; and triaxial tests (with a constant cell pressure) determine material properties for the linear analyses.

HYDROSTATIC COMPRESSION TEST

In a hydrostatic compression test a hydrostatic, isotropic stress is applied (Figure 2(a)) and the change in volume of the sample is recorded. The soil particles are assumed to be incompressible and volume changes are determined by monitoring the amount of pore water expelled from the test specimen into a 10-mℓ pipette. This indicates the compressibility of the material. For this case, the Mohr circle is a point on the normal stress axis (Figure 2(b)); this indicates that the major and minor principal stresses, σ_1 and σ_3, are equal and thus no point within the soil mass is experiencing a shear stress. This is further shown by the horizontal stress path (Figure 2(c)) where the maximum shear stress, q, is zero. Typical test results are shown in Figure 2(d). The slope of the hydrostatic compression curve is the instantaneous bulk modulus, which is plotted as a function of the stress (Figure 2(e)).

CONSTANT MEAN NORMAL STRESS TEST

The constant mean normal stress test is performed by applying hydrostatic stress on the test specimen and then simultaneously decreasing the lateral stress, σ_3,

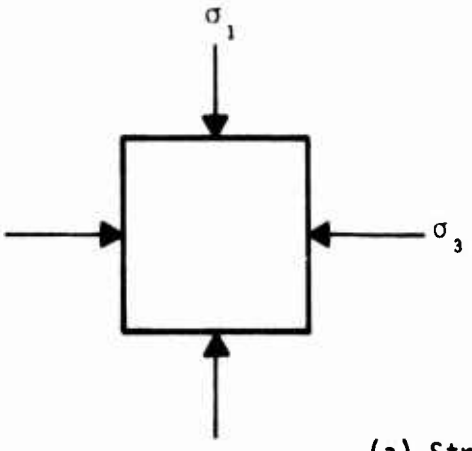

$\sigma_h = \sigma_1 = \sigma_3$

$\varepsilon_v = \varepsilon_1 + \varepsilon_2 + \varepsilon_3,\ \varepsilon_2 = \varepsilon_3$

$\varepsilon_v = \varepsilon_1 + 2\varepsilon_3$

(a) Stress Conditions

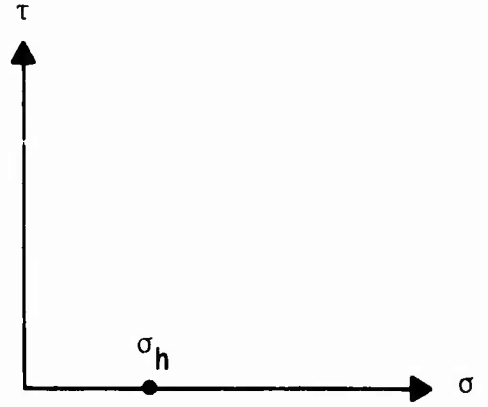

(b) Mohr Circle

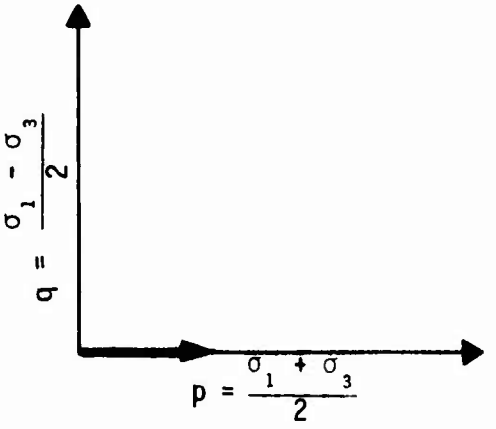

(c) Stress Path

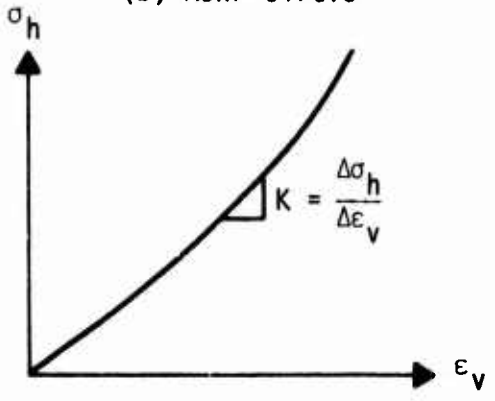

(d) Hydrostatic Compression Curve

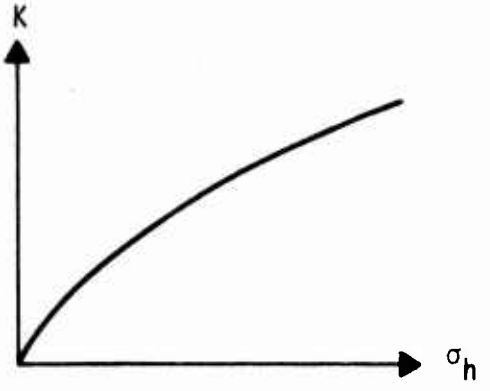

(e) Test Results

Figure 2. Hydrostatic Compression Test Method

and increasing the vertical stress, σ_1. Mean normal stress is defined as

$$\sigma_m = \frac{1}{3}(\sigma_1 + \sigma_2 + \sigma_3)$$

In the triaxial testing apparatus, $\sigma_2 = \sigma_3$ and the mean normal stress becomes

$$\sigma_m = \frac{1}{3}(\sigma_1 + 2\sigma_3)$$

It can be seen from the above equation that σ_m is a constant when the vertical stress, σ_1, is increased twice as much as the lateral stress, σ_3, is decreased; i.e., σ_3 decreases by an increment equal to one half the incremental increase of σ_1, or $\Delta\sigma_1 = -2\Delta\sigma_3$. The sample is first hydrostatically stressed and then the test procedure begins. The sum of the vertical and lateral stresses at any point during the test is equal to the hydrostatic stress initially placed on the sample (Figure 3(a)). Mohr circles are shown in Figure 3(b) for the test at one value of mean normal stress. Similar circles would result at higher hydrostatic and mean normal stresses. Figure 3(c) shows the stress path with a slope of 3:1. The slope indicates that the sample is experiencing greater changes in shear stresses than in normal stresses. Based on limitations in the nature of the triaxial test apparatus, this is the closest to a pure shear condition (of a soil) that can be attained. For the case of pure shear, the slope of the stress path would be vertical. Typical test results are plotted as shear modulus versus mean normal stress (Figure 3(d)). Shear modulus versus mean normal stress is plotted in Figure 3(e).

To determine the shear modulus, both volumetric and vertical strain measurements of the sample must be made. Based on elastic relationships, the shear modulus can be expressed as

$$G = \frac{E}{2(1 + \mu)} \tag{1}$$

and the modulus of elasticity, E, is defined as

$$E = \frac{\Delta(\sigma_1 - \sigma_3)}{\Delta\varepsilon_1} \tag{2}$$

where $\Delta(\sigma_1 - \sigma_3)$ is the principal stress difference and ε_1 is the vertical strain of the sample.

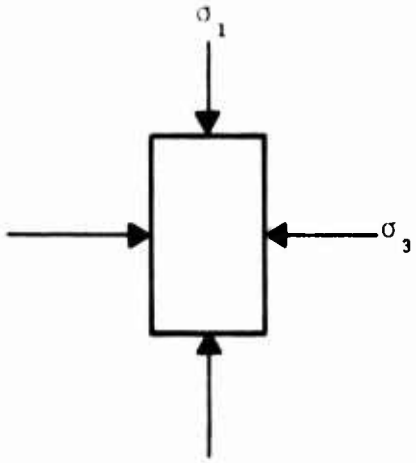

$$\Delta\sigma_3 = -\frac{\Delta\sigma_1}{2}$$

$$G = \frac{\Delta(\sigma_1 - \sigma_3)}{3\varepsilon_1 - \varepsilon_v}$$

(a) Stress Conditions

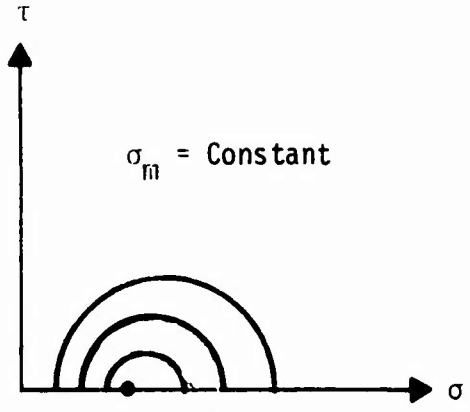

(b) Mohr Circles

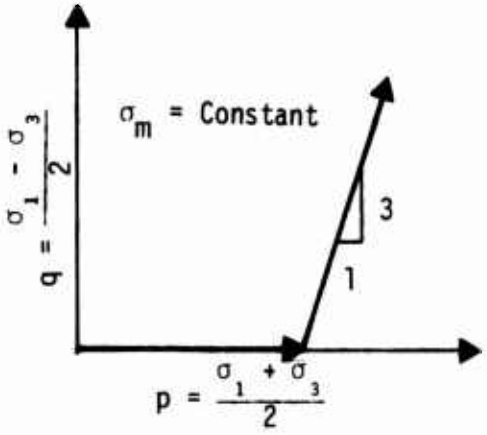

(c) Stress Path

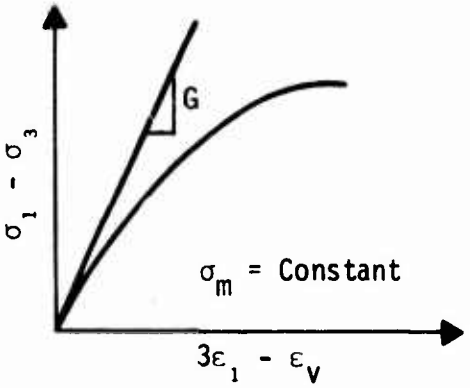

(d) Constant Mean Normal Stress Curve

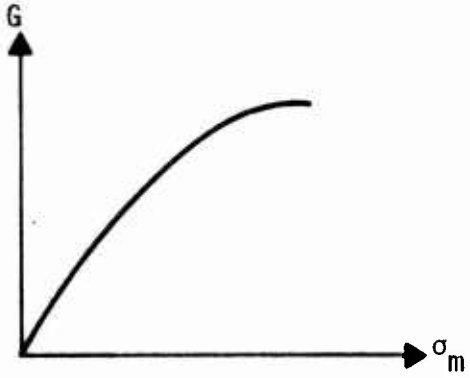

(e) Test Results

Figure 3. Constant Mean Normal Stress Test Method

If Equation (2) is substituted into Equation (1),

$$G = \frac{\Delta(\sigma_1 - \sigma_3)}{2(1 + \mu)\varepsilon_1} \tag{3}$$

But Poisson's ratio, μ, can be expressed as

$$\mu = \frac{\varepsilon_2}{\varepsilon_1} \tag{4}$$

and the volumetric strain, ε_v, is the sum of the principal strains

$$\varepsilon_v = \varepsilon_1 + \varepsilon_2 + \varepsilon_3 \tag{5}$$

and then $\varepsilon_2 = \varepsilon_3$ is applicable to the triaxial apparatus. Thus,

$$\varepsilon_v = \varepsilon_1 + 2\varepsilon_3 \tag{6}$$

If compressive strains are considered positive, Equation (6) becomes

$$\varepsilon_v = \varepsilon_1 - 2\varepsilon_3 \tag{7}$$

Since lateral strains are not normally measured in the triaxial apparatus, Equation (7) is slightly modified and substituted into Equation (3) with Equation (4).

$$\varepsilon_3 = \frac{\varepsilon_1 - \varepsilon_v}{2}$$

Then

$$G = \frac{\Delta(\sigma_1 - \sigma_3)}{2\left(1 + \frac{\varepsilon_3}{\varepsilon_1}\right)\varepsilon_1} = \frac{\Delta(\sigma_1 - \sigma_3)}{3\varepsilon_1 - \varepsilon_v} \tag{8}$$

Equation (8) is used to determine the shear modulus for each magnitude of the mean normal stress. Volumetric and vertical strains are positive for a decrease in sample volume and neight. If the sample volume increases--indicated by pore water being drawn into the sample--the volumetric strain is added to $3\varepsilon_1$; if the sample volume decreases--indicated by expelled pore water--the volumetric strain is subtracted from $3\varepsilon_1$.

TRIAXIAL TEST

Because the BDR Code uses the bulk and shear moduli as a function of strain, it was decided that any substitute soil parameters should be ones which could be used to calculate these parameters. Plate-bearing and penetrometer tests were eliminated from consideration because the data from these tests cannot be directly related to the volume-change characteristics of a soil. Also, the selected test should be as simple as possible so that it could be performed with various materials in standard laboratories. Based on these considerations, the standard triaxial compression test was selected.

In a triaxial test, a cylindrical sample is prepared and placed in a rubber membrane in a triaxial-loading apparatus. The sample does not have to be saturated, but drainage must be provided to eliminate pore pressure. A consolidation (hydrostatic) stress is applied to the sample and the sample is allowed to reach equilibrium (Figure 4(a)). The vertical stress, σ_1, is then increased until failure occurs, while the lateral stress, σ_3, is held constant. Mohr circles and the stress path for the test are shown in Figure 4(b) and (c), respectively. Vertical deformation measurements are recorded as well as the vertical and lateral stresses for subsequent data reduction. The principal stress difference, $\Delta(\sigma_1 - \sigma_3)$, is plotted against the vertical strain, ε_1, and the slope of the curve is the modulus of elasticity, E (Figure 4(d)). The test is repeated for a greater lateral stress and a new initial tangent modulus is computed. The end result is a plot of E versus σ_3 (Figure 4(e)). Once the modulus of elasticity is known, the bulk and shear moduli can be calculated by assuming a Poisson's ratio for the test material (Reference 4) and using the following equations, which are based on elastic theory:

$$K = \frac{E}{3(1 - 2\mu)}$$

$$G = \frac{E}{2(1 + \mu)}$$

---

4. Bowles, Joseph E., *Foundation Analysis and Design*, McGraw-Hill, New York, 1968.

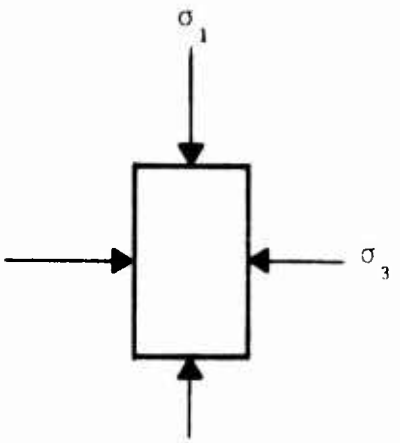

(a) Stress Conditions

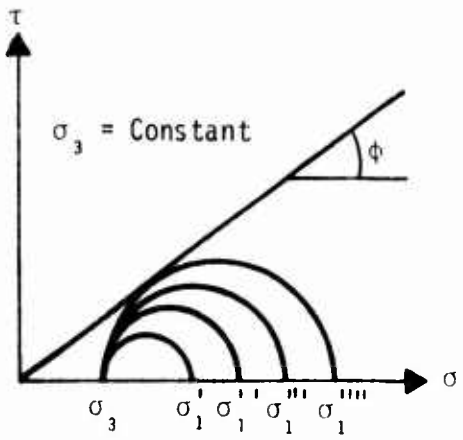

(b) Mohr Circles

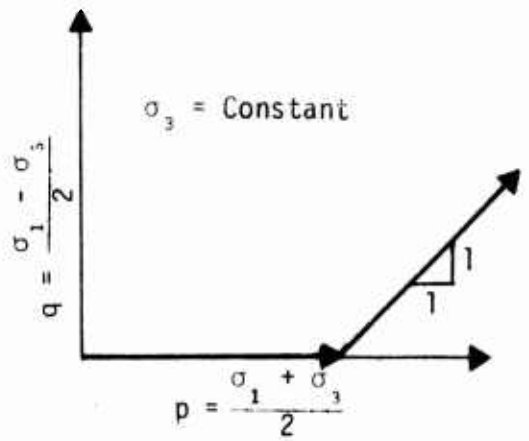

(c) Stress Path

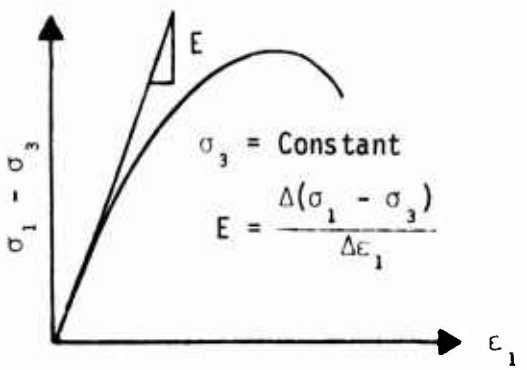

(d) Triaxial Compression Curve

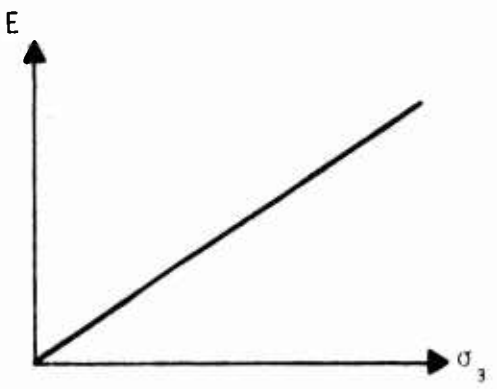

(e) Test Results

Figure 4. Standard Triaxial Compression Test Method

SUMMARY

The bulk and shear moduli determined from hydrostatic and mean normal stress tests provide the data for an exact nonlinear analysis. Use of the triaxial test to determine an elastic modulus from which shear and bulk moduli can be calculated comprises an approximate linear analysis. Thus, BDR crater performance with nonlinear and linear material parameters can be compared.

SECTION IV
LABORATORY TESTING

Laboratory testing was not originally included in this project. However, a detailed literature search for strength data on BDR materials which had been tested in hydrostatic compression, constant mean normal stress, and triaxial compression was unsuccessful. Therefore, the required data had to be collected at the CERF facility.

MATERIALS

The materials selected for testing were (1) a concrete sand, (2) a 3/8-inch-diameter pea gravel, (3) a 3/4-inch-diameter gravel, and (4) a well-graded crushed limestone (Figure 5). Materials (1), (2), and (3) were selected because of their availability around the world and their potential use in BDR; the crushed limestone was selected because it was used as a base course material in the BDR field studies at Tyndall Air Force Base, Florida (Reference 5).

SAMPLES

Conventional laboratory procedures for testing granular soils with the triaxial cell apparatus (Reference 6) involve placing the soil in a thin rubber membrane and placing a vacuum on the sample until the chamber fluid can create a lateral stress to retain the shape of the sample. However, when a thin rubber membrane is used with granular soils containing large particles, membrane puncture becomes a problem. The sample preparation procedure was thus modified by first preparing the sample in a standard 4-inch-diameter Proctor compaction mold split

---

5. Hokanson, Lawrence D., *Tyndall AFB Bomb Damage Repair Field Test, Documentation and Analysis*, AFWL-TR-74-226, Air Force Weapons Laboratory, Kirtland Air Force Base, New Mexico, October 1975.

6. Bishop, Alan W., and Henkel, D. J., *The Measurement of Soil Properties in the Triaxial Test*, Edward Arnold Ltd., London, 1957.

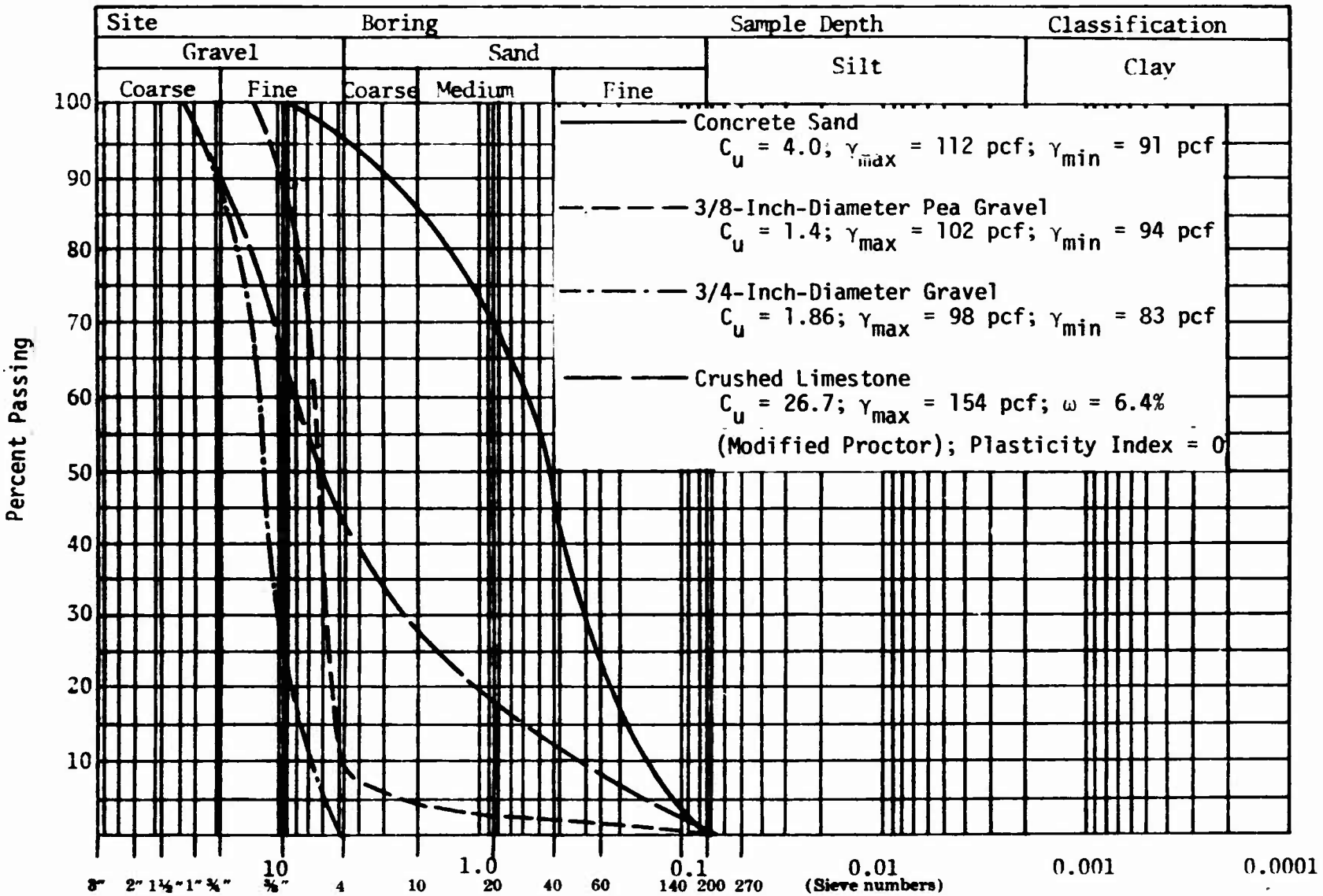

Figure 5. Gradation Curves for Fill Materials

along its side. Rubber membranes were placed around the outside of the mold to prevent the escape of water from the sample and a hose clamp was used to keep the mold together. The sample was then saturated and frozen (Figure 6). The frozen sample was easily removed from the split mold (Figure 7), placed into the triaxial apparatus, and allowed to thaw over night. Membrane puncture was avoided by using a Hveem Stabilometer as the testing apparatus.

EQUIPMENT AND SETUP

The Hveem Stabilometer was originally intended to be used in testing subgrade, base-course, and surface-pavement materials to determine the *resistance value* of the material (Reference 7). Hveem Stabilometer membranes are approximately 0.09-inch thick, thereby reducing considerably the danger of membrane puncture. (Standard membranes are approximately 0.01-inch thick.) Lateral hydraulic pressure is generated by the hand pump on the stabilometer. This pressure is monitored by a gage mounted on the side of the stabilometer and connected to the fluid chamber between the frame and the membrane. Lateral pressure is increased by displacing fluid from a reservoir into the fluid chamber. Vertical stress is applied by a standard compression machine and monitored with a proving ring.

Because pore water volume changes are not taken in the standard test procedure with the stabilometer (Reference 7), it was necessary to design platens for both ends of the sample to prevent the escape of pore water. These aluminum platens were 4 inches in diameter by 0.5-inch thick. A groove was made along the circumference to accept an O-ring which created a watertight seal with the stabilometer membrane. Drainage of the sample was made possible by connecting 3/8-inch-diameter tubing to both the lower and upper platens. A water supply connected to the lower platen allowed for saturation of the sample. During testing, the upper drainage outlet (platen) was closed and the expelled pore water exited the sample through the lower drainage outlet to a 10-mℓ pipette for volume

---

7. Horonjeff, Robert, and Jones, John H., *The Design of Flexible and Rigid Pavements*, University of California Press, Berkeley and Los Angeles, California, 1953.

Figure 6. Frozen Sample in Standard Proctor Compaction Mold

Figure 7. Frozen Sample of 3/4-Inch-Diameter Gravel

measurement. The platens, stabilometer, and loading ram are shown in Figure 8; the test setup is shown in Figure 9.

TEST RESULTS

Results from the hydrostatic compression test series on the four fill materials are shown in Figure 10. The 3/4-inch-diameter gravel can be considered to be in a medium dense state. The compaction effort consisted of tamping the sample in layers. Dense samples of pea gravel and sand were obtained by vibration. The crushed limestone was compacted at an optimum water content of 6.4 percent (Figure 11) as determined by ASTM D1557, Method D, using a 6-inch-diameter mold. The curves presented are the result of a minimum of three tests and the density given is an average density of the three samples. It can be seen from these plots that the compressibility decreases, for uniformly graded materials, with decreasing particle size; increasing the density of a particular material has a similar effect on the compressibility. This is especially well illustrated in Figure 12, which shows the effect of density on the compressibility of the well-graded crushed limestone material.

Because the stabilometer is not usually used as a triaxial cell for testing soils and recording pore water volume changes, a comparison of stabilometer results and conventional triaxial cell data was necessary. CERF data on a local sand and the results of NCEL tests on sand were used for this purpose. These sands were similar and both are used commercially in concrete production. Figure 13 shows the NCEL gradation curve for the sand. Figure 14 shows the hydrostatic compression data for these sands in the loose and dense states. The NCEL curves were prepared by calculating the volumetric strain from the data in Table 1(Reference 8). The difference in the gradation of the sands and its effect on the compressibility of the material were considered minor. Calculation

---

8. Forrest, James B., and Shugar, T. A., *A Structural Evaluation of Rapid Methods of Backfilling for Bomb Damage Repair*, AFWL-TR-73-29, Air Force Weapons Laboratory, Kirtland Air Force Base, New Mexico, March 1974.

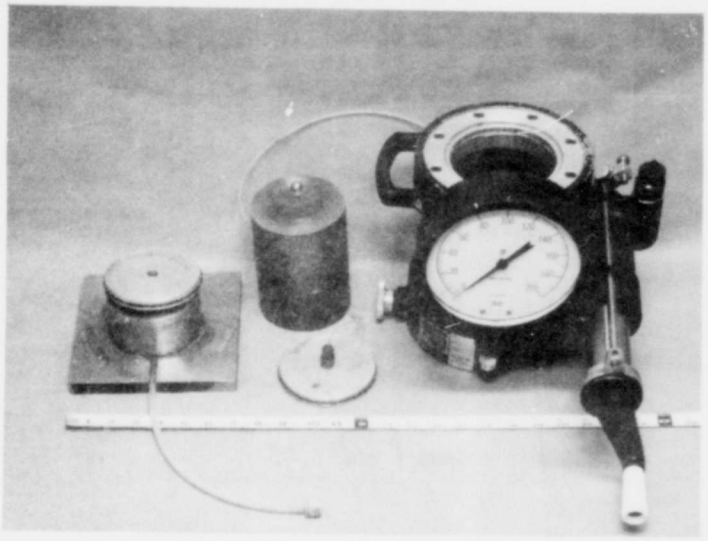

Figure 8. Hveem Stabilometer and CERF-Designed Equipment

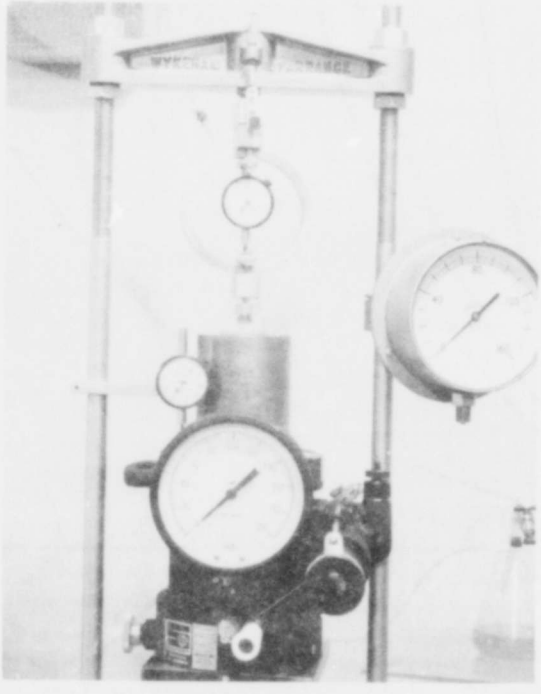

Figure 9. Stabilometer Test Setup

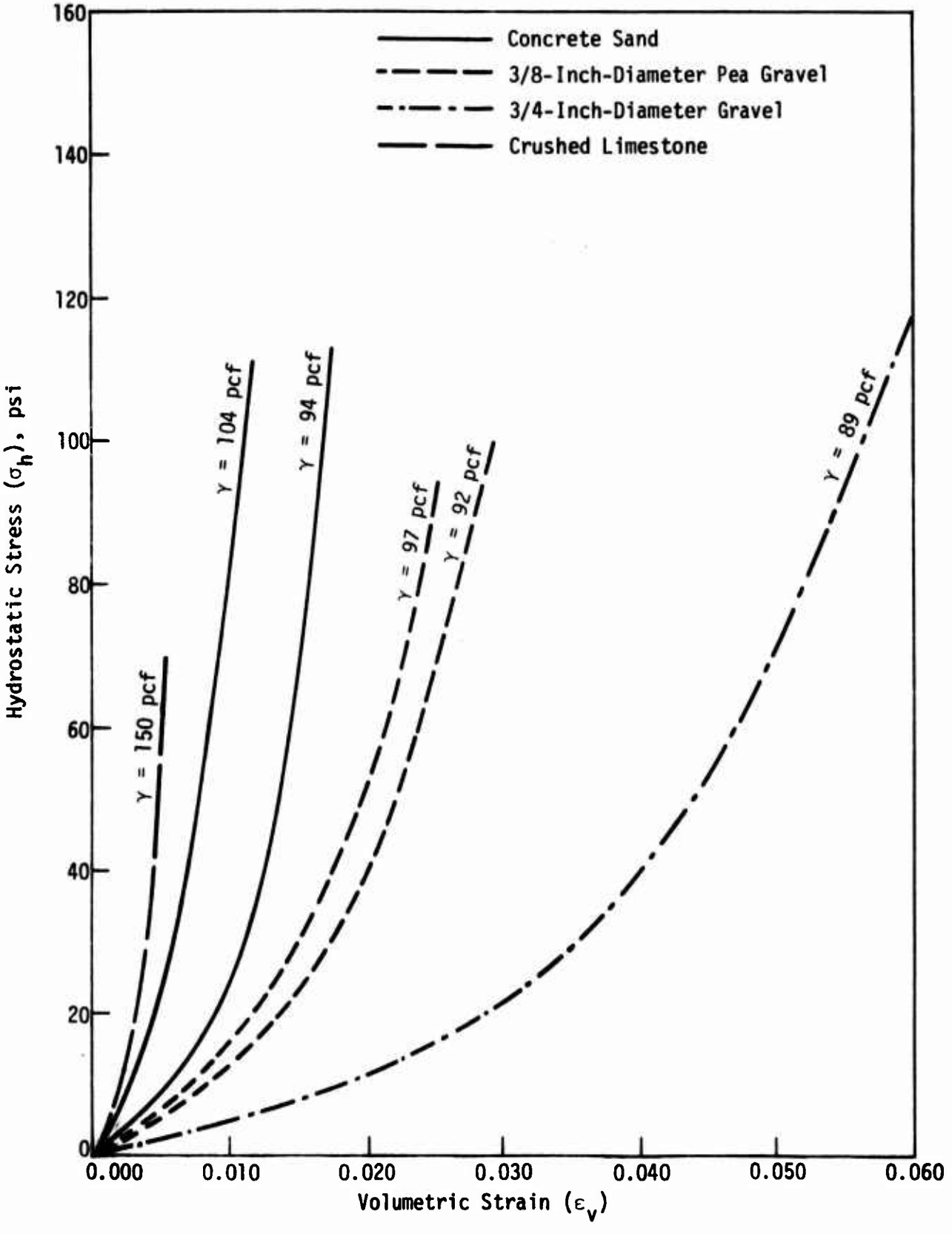

Figure 10. Hydrostatic Compression Test Data

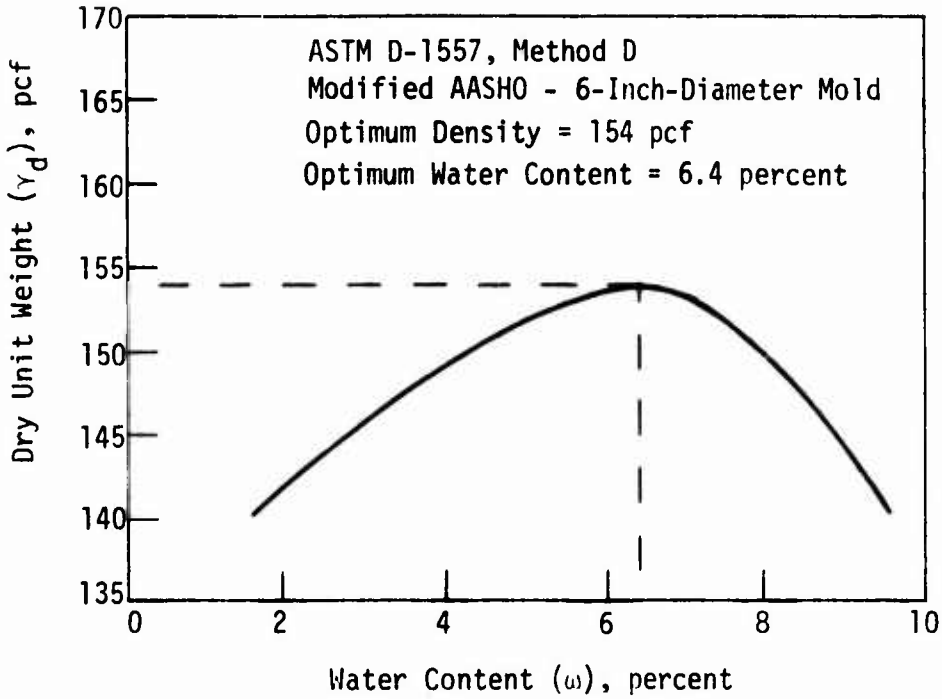

Figure 11. Moisture/Density Curve for Crushed Limestone

of volumetric strains from the NCEL data introduces error into the curves and makes the samples appear more compressible than they actually are; therefore, the NCEL data should be shifted to the left slightly to better agree with the CERF data with respect to density. Thus it appears that similar results can be obtained from the stabilometer and the conventional triaxial cell apparatus.

The shear moduli computed from the constant mean normal stress tests are shown in Figure 15. A significantly higher NCEL shear modulus is seen for the dense sand (γ_d = 108 pcf) than for the loose sand (γ_d = 96.6 pcf). The CERF shear moduli for the sand appear to be consistent with the densities of the samples. Based on the results of the tests, the shear modulus is dependent on the gradation and the density of the material. The dense sand (NCEL data) has a much higher shear modulus than the 3/4-inch-diameter gravel. The crushed limestone has intermediate shear moduli because it is a well-graded material containing a high percentage of large particles as well as fine. Because of the uniform gradation of rounded particles, there was no significant difference in shear moduli between the loose and dense pea gravel samples.

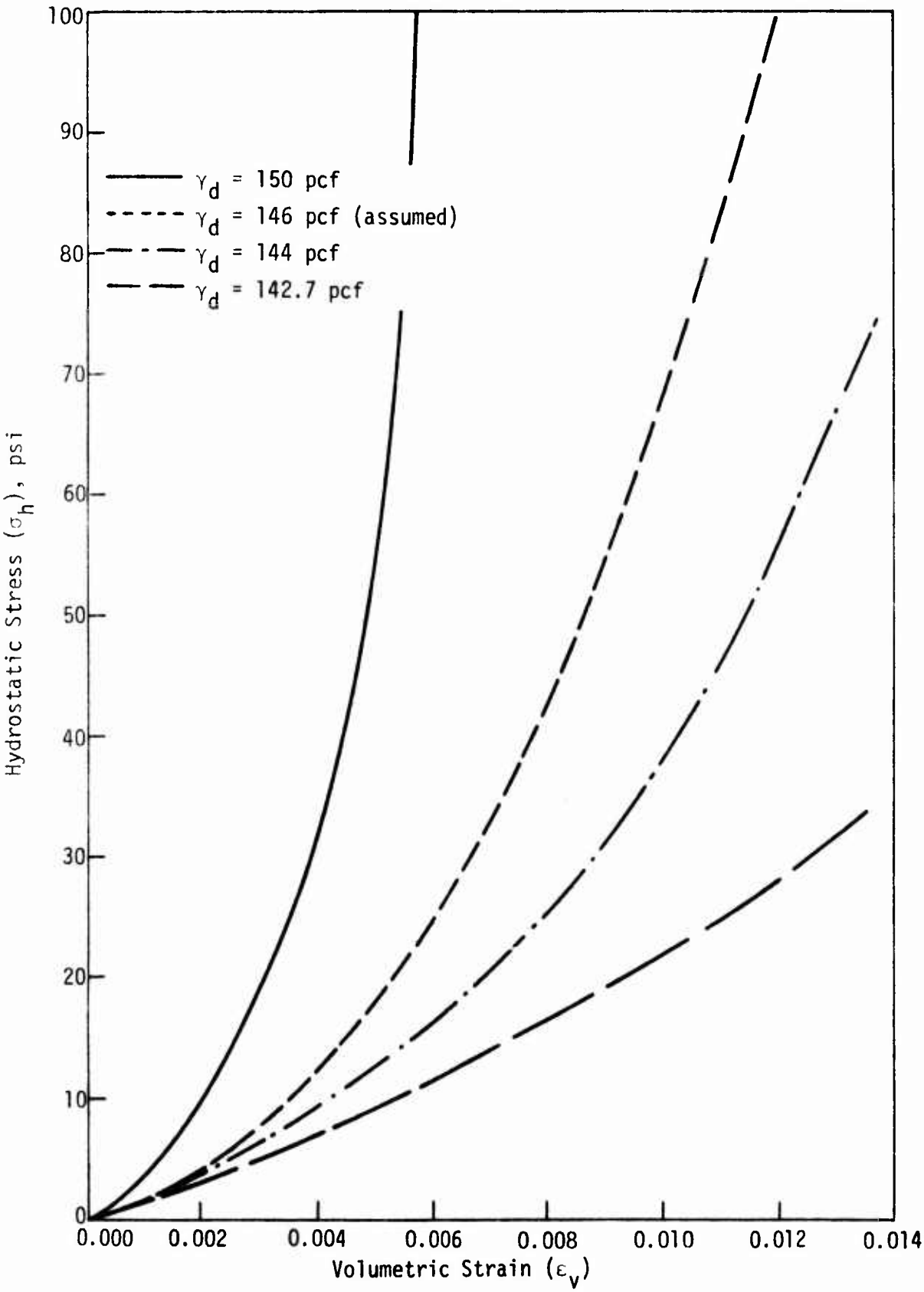

Figure 12. Hydrostatic Compression Test Data for Crushed Limestone at Various Densities

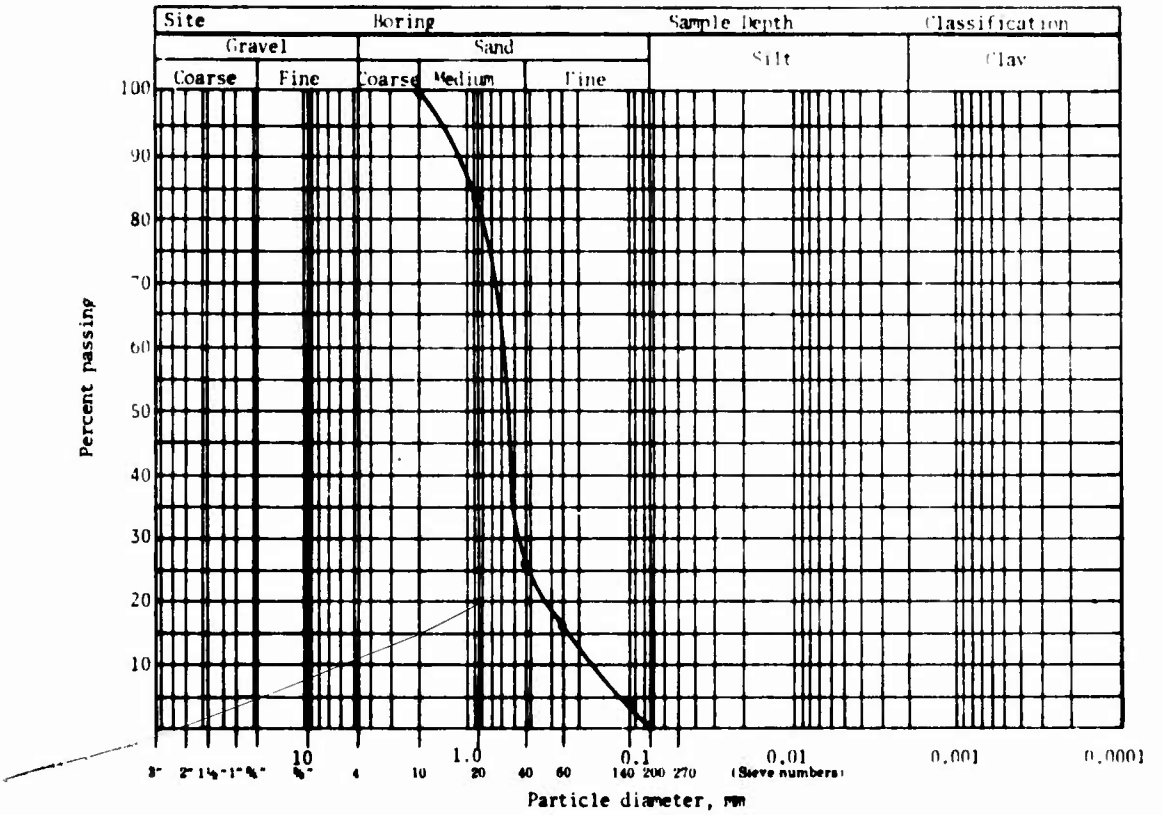

[after Forrest (Reference 8)]

Figure 13. NCEL Gradation Curve for Sand

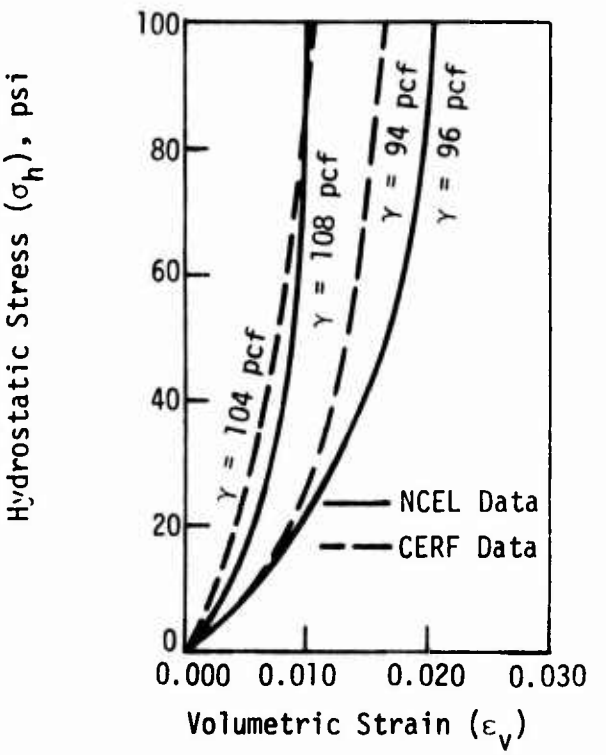

Figure 14. Hydrostatic Compression Test Data for Sand in Loose and Dense States

TABLE 1. NCEL TEST RESULTS ON SAND

Confining Stress (psi)	Bulk Modulus Loading K (psi)	Bulk Modulus Unloading K_u (psi)	Shear Modulus G (psi)
Compacted			
0	2,800	-	400
5	2,900	7,000	1,200
10	3,000	7,000	2,200
15	3,400	7,000	4,000
20	4,600	7,000	5,600
25	6,500	9,000	7,600
30	7,800	9,000	9,200
35	9,200	9,000	10,400
40	10,800	11,000	11,000
45	12,600	12,600	11,500
Loose			
0	1,600	-	200
5	1,700	4,000	500
10	1,900	4,000	800
15	2,200	4,000	1,400
20	2,400	5,000	2,000
25	3,000	5,000	2,800
30	3,700	6,000	3,500
35	4,500	6,000	4,000
40	5,000	6,000	4,200
45	5,300	8,000	4,400

[after Forrest (Reference 8)]

The last set of data (Figure 16) shows the results of standard triaxial compression (constant lateral stress) tests on the four fill materials. The 3/4-inch-diameter gravel was tested only in a dense state. Only one curve is shown for the pea gravel because the data for loose and dense samples were not significantly different. The crushed limestone (γ_d = 150 pcf) had a response very similar to that of the dense sand (γ_d = 104 pcf). This is a very good illustration of the effect of separating a general state-of-stress into volumetric and shear components. Results of the hydrostatic compression tests (Figure 10) show the crushed limestone to be less compressible than the dense sand. However, the shear moduli (Figure 15) for the crushed limestone are less than those for dense sand. When the same load, or stress, is applied to the two materials, as in the triaxial compression test, similar material behavior results. The high bulk moduli and the low shear moduli of the crushed limestone create the same material response as a low bulk moduli and a high shear moduli.

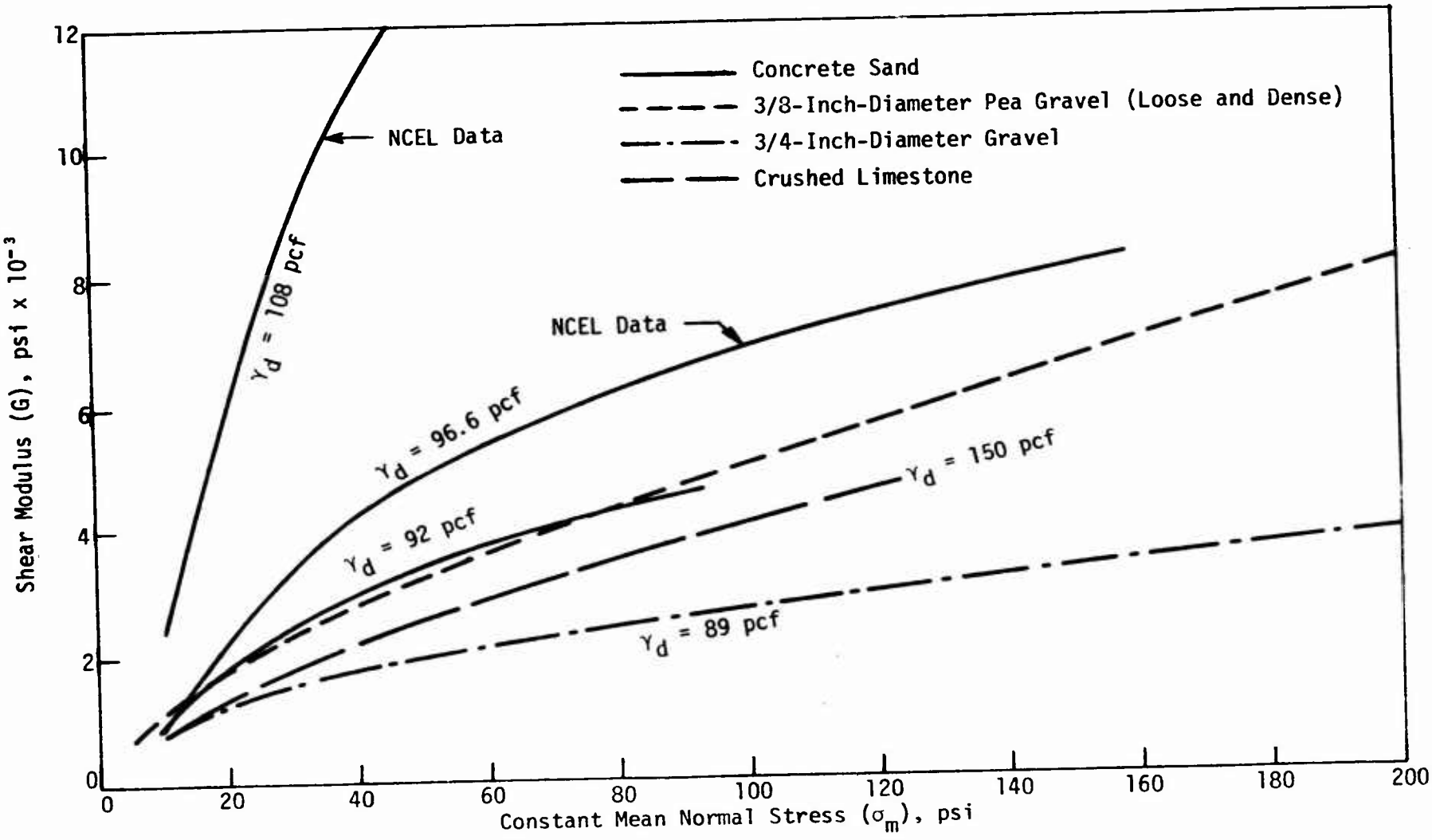

Figure 15. Constant Mean Normal Stress Test Data

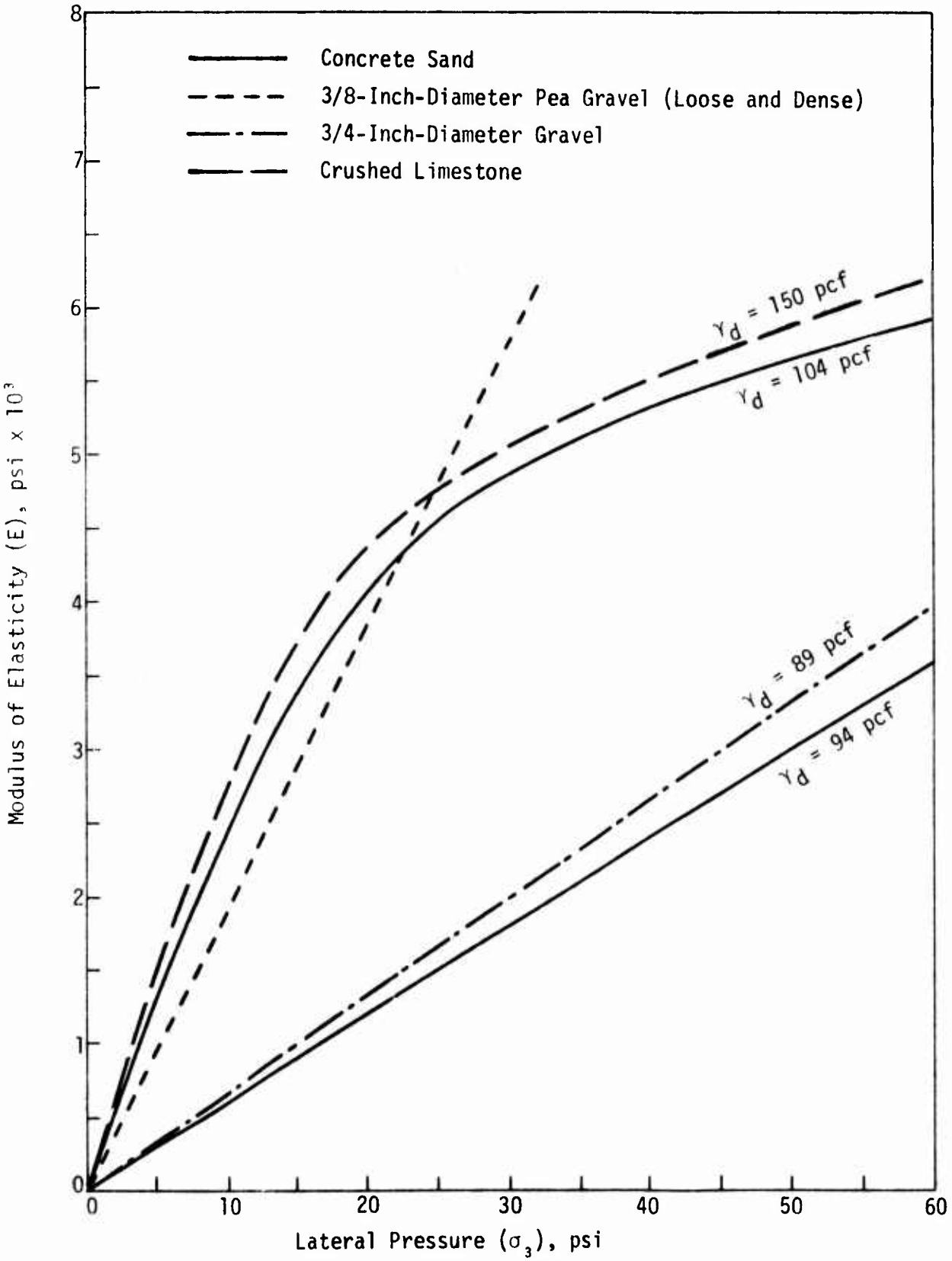

Figure 16. Standard Triaxial Compression Test Data

SECTION V
COMPUTER ANALYSIS

COMPUTER CODE

The Bomb Damage Repair (BDR) Code is a finite-element code consisting of three programs: GEN2D, WINDAX, and PLOT2D.

GEN2D, the finite-element mesh generator, has two options: either a minimum amount of the crater's mesh geometry can be inputted and the computer will generate intermediate nodal points and elements, or all the element and nodal data obtained from a scaled drawing of the crater mesh--nodal points, coordinates, element definitions, and material identifications--can be inputted. The latter method is only used if a detailed model of the crater profile is desired. Analyses which have been made with detailed and approximate crater profiles (References 8, and 9) indicate that detailed modeling does not contribute significantly to the accuracy of the results.

WINDAX is the problem-solving program of the code. Material properties and loading criteria (input to WINDAX) are used to compute stresses, strains, and deflections (printed output) for a particular BDR crater. The results from WINDAX are used to analyze the crater mesh input (e.g., mesh dimensions, boundary conditions, and stresses) for accurate modeling of the field conditions. (This is largely dependent on the user's experience with finite-element programs.) The procedure is continued until the computer input models the field conditions as closely as possible. WINDAX output is then used to evaluate the crater's response to different loading conditions.

PLOT2D is the plotting routine[a] which graphically illustrates the output of

---

9. Crawford, John, and Forrest, James B., *A Structural Evaluation of Rapid Methods of Backfilling for Bomb Damage Repair*, AFWL-TR-74-272, Air Force Weapons Laboratory, Kirtland Air Force Base, New Mexico, August 1975.

[a]This program was not used in this project because all the data necessary for evaluation of the performance of a BDR crater (e.g., deflection) was supplied by WINDAX and also because the program cannot presently be run with the computer software at the AFWL computer center.

GEN2D or WINDAX for interpretation of the crater system, and it is very useful in designing and selecting an appropriate mesh for BDR crater problems. References 8 and 9 indicate that the crater profile can be approximated with a generated mesh from GEN2D without introducing significant errors into the computed results of WINDAX. A number of different finite-element meshes can be generated by GEN2D and plotted by PLOT2D, and the one which models the crater profile best can be selected.

CRATER MODEL

The finite-element mesh used in this study was an exact model of Crater 1-2, which had been created for the BDR field study at Tyndall Air Force Base, Florida (Reference 5). The surface material was AM2 landing mat, which is presently used in BDR work. Directly beneath this matting was a zone containing one of the four fill materials selected for this study. The mesh was designed so that this fill zone could be varied (12, 18, or 24 inches). Because the materials immediately below the fill zone undergo a small amount of compaction due to the trafficking of backfill equipment, a zone of compacted pushback[a] material was assumed. The data presented in Table 2 were used to calculate the stress/strain curves for the crater wall and the fallback debris; the properties of the compacted pushback material were assumed to lie between those of these two materials. In addition to these crater zones, zones of fallback debris and uncompacted pushback material, disturbed in-situ soil (crater wall), and undisturbed in-situ soil were established. Concrete pavement sections equivalent in volume to that in the Tyndall crater (approximately 40 percent of ejecta) were located within the crater mesh. Figure 17 shows the finite-element mesh with the apparent and true crater profiles, and the approximation of the crater profile; the detailed model is shown in Figure 18.

An F-4E aircraft with a tire pressure of 265 psi and a tire-print area of 102 in^2 (total load = 27,000 lb) was used for analysis and inputted to the BDR Code. The rectangular tire-print area was converted to an equivalent circular plate of 5.7-inch radius.

---

[a]The term *pushback*, as used here, means *replaced crater ejecta*.

TABLE 2. MATERIAL CHARACTERISTICS FOR SILTY CLAY FROM KANSAS CRATERS

Confining Stress (psi)	Bulk Modulus Loading K (psi)	Bulk Modulus Unloading K_u (psi)	Shear Modulus G (psi)
Crater Wall			
0	8,000	--	700
5	8,500	30,000	900
10	9,800	30,000	1,300
15	11,800	30,000	2,000
20	14,000	30,000	3,100
25	17,000	30,000	3,800
30	21,200	30,000	4,300
35	25,800	30,000	4,700
40	30,000	30,000	5,000
45	32,000	30,000	5,200
Fallback Debris			
0	3,000	--	200
5	3,000	10,000	300
10	3,200	10,000	500
15	3,400	10,000	1,100
20	4,000	10,000	1,500
25	4,800	10,000	1,800
30	5,500	10,000	2,200
35	6,200	10,000	2,900
40	7,200	10,000	3,900
45	8,600	10,000	4,800

[after Forrest (Reference 8)]

ANALYTICAL PROCEDURE

The data obtained from the laboratory tests were used as input to the BDR Code in two types of analyses. First, an analysis was performed with the nonlinear material properties determined from the hydrostatic compression test and the constant mean normal stress test. This consisted of defining a piecewise linear stress/strain curve with five segments. The bulk modulus, K, for a particular volumetric strain, ε_v, and the shear modulus, G, for the corresponding mean normal stress, σ_m, for six different strains along the hydrostatic compression curve were inputted to WINDAX. These data were used to calculate a stiffness matrix (References 8 and 9) to predict the response of the elements to a particular

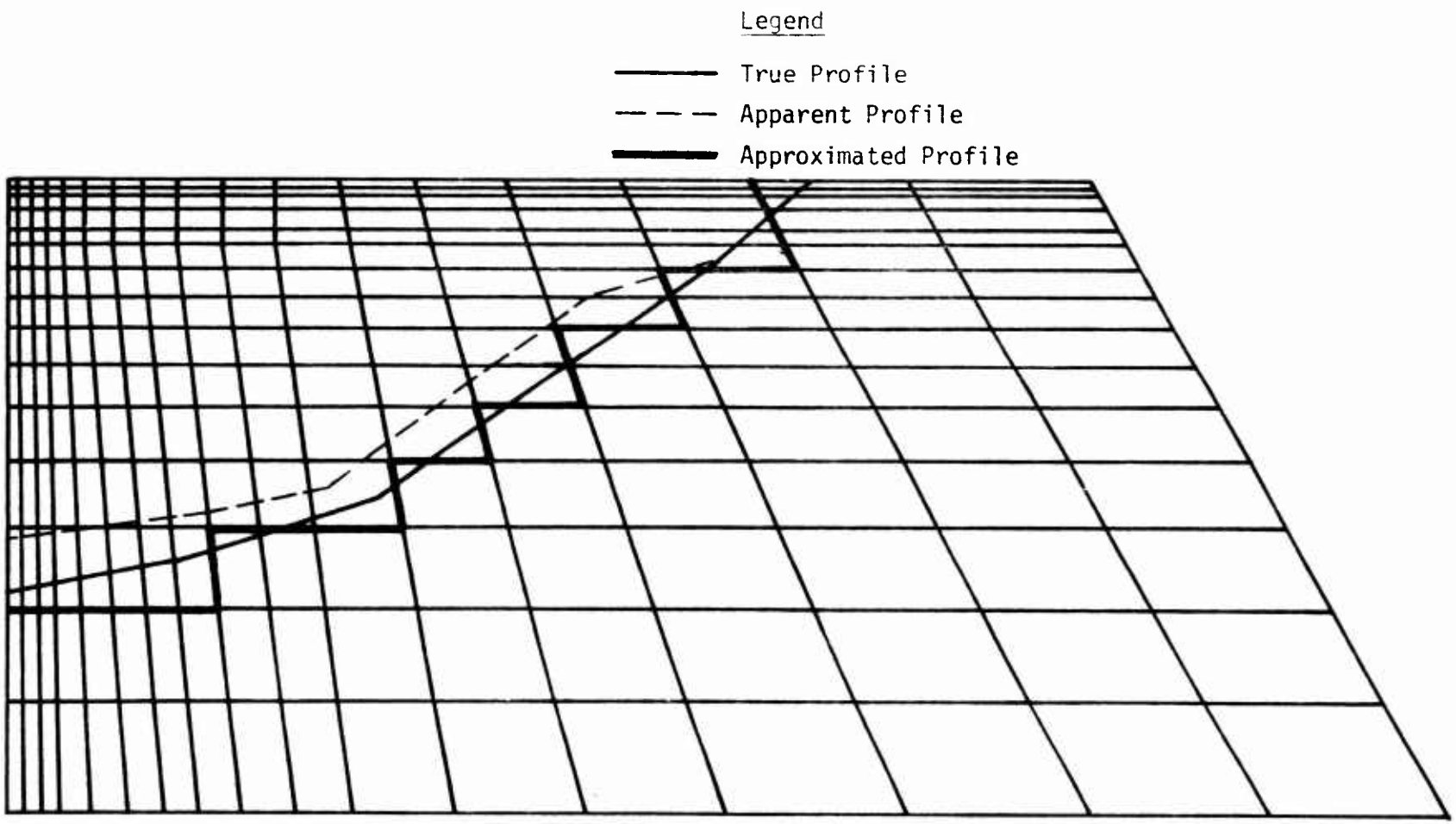

Figure 17. Finite-Element Mesh with Crater Profiles

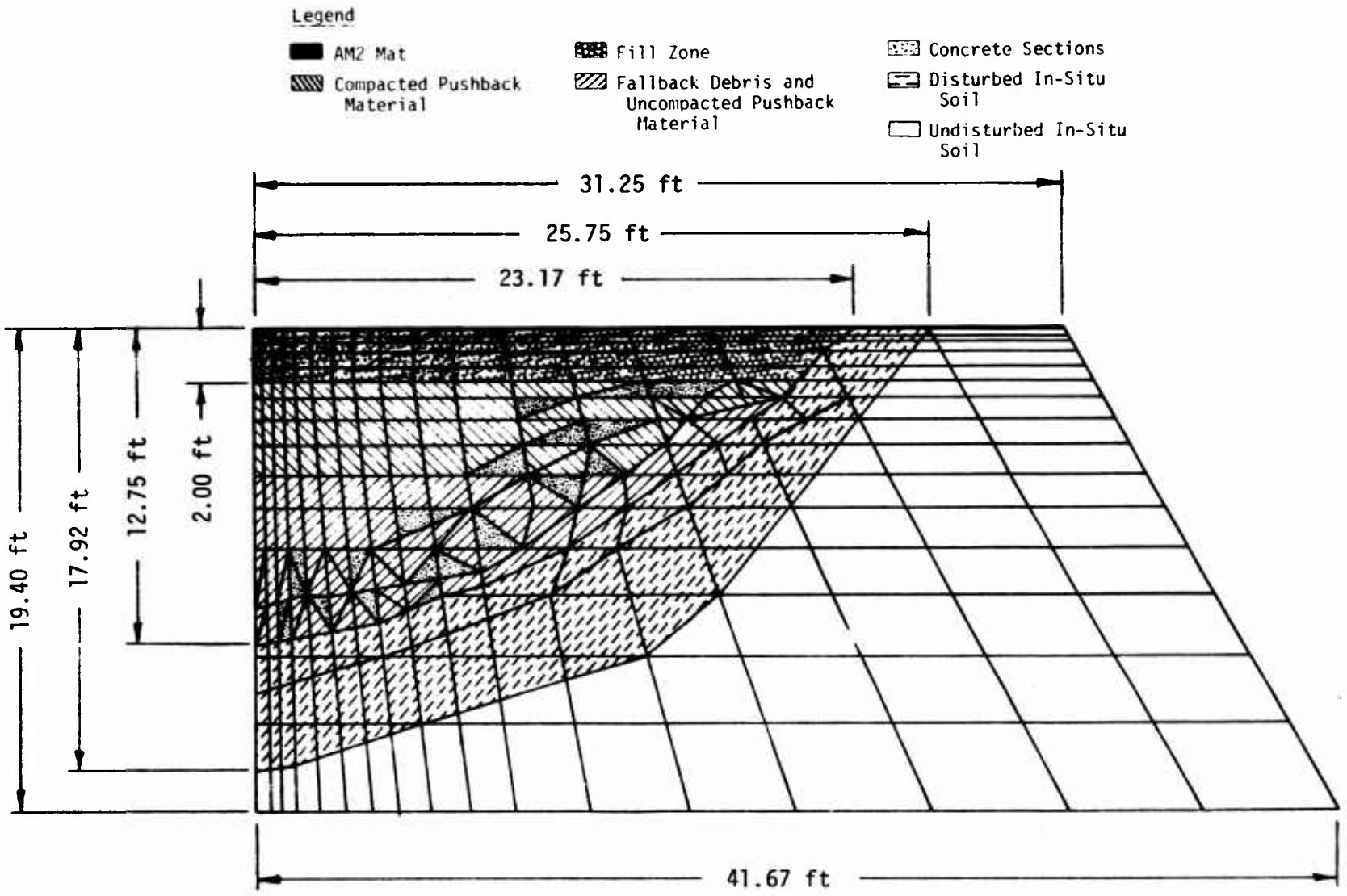

Figure 18. Detailed Model of Crater

load. In the second analysis, the bulk and shear moduli determined by

$$K = \frac{E}{3(1 - 2\mu)}$$

and

$$G = \frac{E}{2(1 + \mu)}$$

were used, where

K = bulk modulus

G = shear modulus

E = modulus of elasticity (determined by triaxial compression test)

μ = Poisson's ratio (assumed)

The modulus of elasticity used was the initial tangent modulus, expressed in terms of the lateral (cell) pressure. Bulk and shear moduli were calculated using an assumed Poisson's ratio. The calculated moduli were inputted to the BDR Code and deflections were computed.

COMPUTED RESULTS

Nonlinear Analysis

Fill Materials--The deflections computed by the BDR Code with the nonlinear material property data are shown in Table 3 for the different thicknesses of fill material. The fill material thickness was varied by changing the material definition of certain elements in the crater mesh. Because of the lack of test data, the compacted pushback material was assumed to be less compressible than the fallback debris and more compressible than the crater wall material. However, test results on the fill materials revealed that these materials were more compressible than the compacted pushback materials. As a result of the assumed stress/strain properties of the compacted pushback material, the computed deflections increased as the thickness of the fill material increased. This indicates that either the properties of the compacted pushback

TABLE 3. COMPUTED DEFLECTIONS FROM NONLINEAR DATA

Material	γ_d, pcf	Deflection, inch		
		12-Inch-Thick Fill	18-Inch-Thick Fill	24-Inch-Thick Fill
Sand (Loose)*	96	0.58	0.71	0.81
Sand (Dense)*	108	0.38	0.43	0.47
Sand (Loose)	94	0.67	0.85	0.98
Sand (Dense)	104	0.53	0.64	0.72
Pea Gravel (Loose)	92	0.67	0.76	0.81
Pea Gravel (Dense)	97	0.62	0.71	0.77
3/4-Inch-Diameter Gravel (Dense)	89	0.86	1.03	1.15
Tyndall Crushed Limestone (Dense)	150			
First Analysis		0.51	0.59	0.66
Second Analysis		0.35	0.34	0.33

*NCEL data.

material were inaccurately assumed,[a] or the materials selected for analysis (i.e., sand and gravels) were in fact more compressible than the compacted pushback material. The latter reason seems unlikely and compacted pushback material properties can only be verified by performing laboratory or field tests.

The deflection basins for the four fill materials are shown in Figure 19 for 12-inch-thick fills; similar curves were obtained for the 18- and 24-inch-thick fills. These computed deflections were approximately twice the measured field deflections on similar materials (Figure 20 and References 10 and 11). It was felt that prediction of actual field deflection measurements was not possible

[a]The assumptions made relative to modeling the compacted pushback material were established in conference with the project officers. Because this project was directed toward demonstrating the usefulness of the NCEL BDR Code, rather than an exercise to establish material properties, the assumed material properties were not revised.

10. Frenick, W. B., *Evaluation of Washington Aluminum Company AM2 Landing Mat*, Miscellaneous Paper No. 4-753, U.S.A.E.W.E.S., Vicksburg, Miss., November 1965.

11. Grau, R. W., *Evaluation of May Two-Piece AM2 Landing Mat*, Miscellaneous Paper No. 5-68-11, U.S.A.E.W.E.S., Vicksburg, Miss., July 1968.

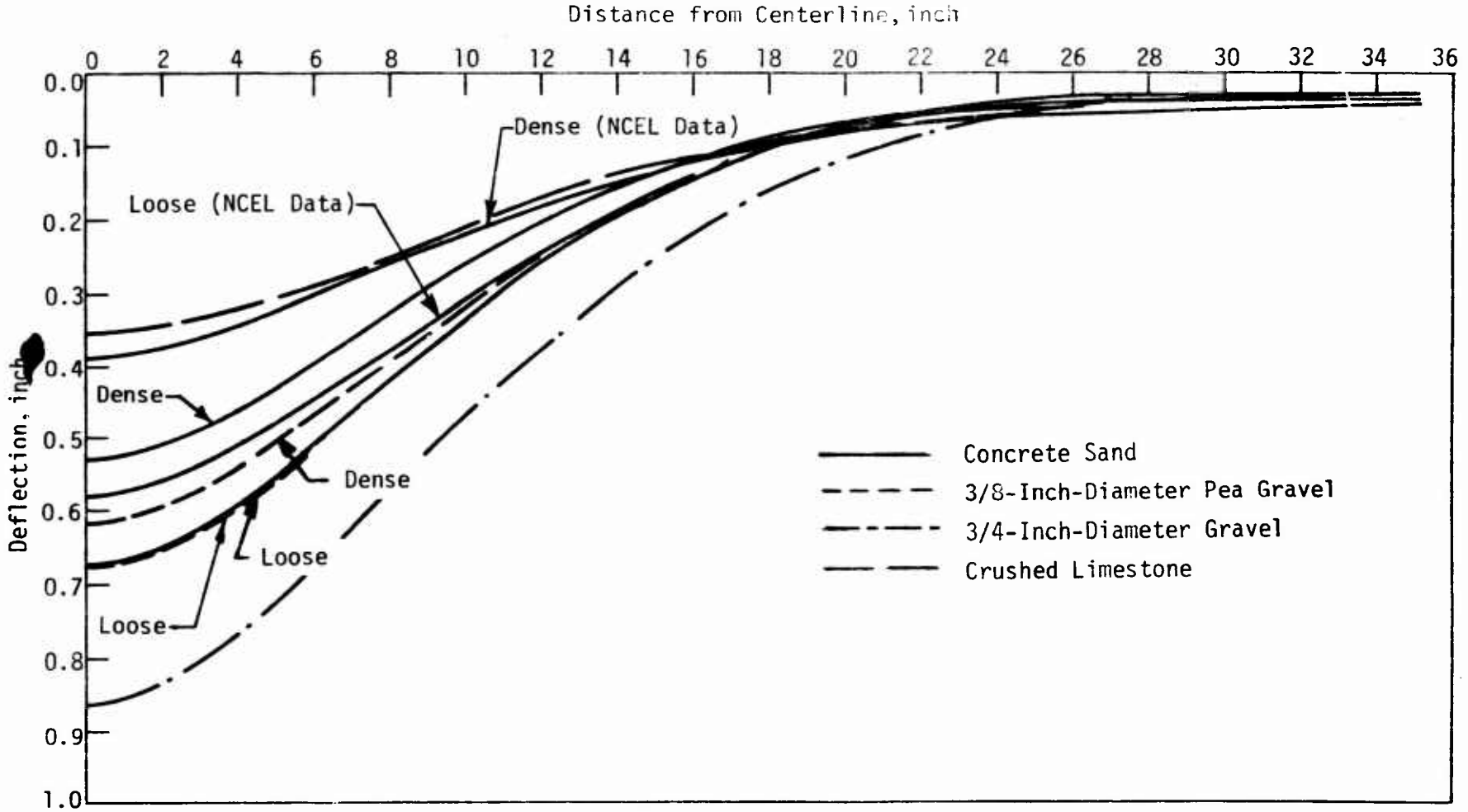

Figure 19. Deflection Basins for 12-Inch-Thick Fill Materials

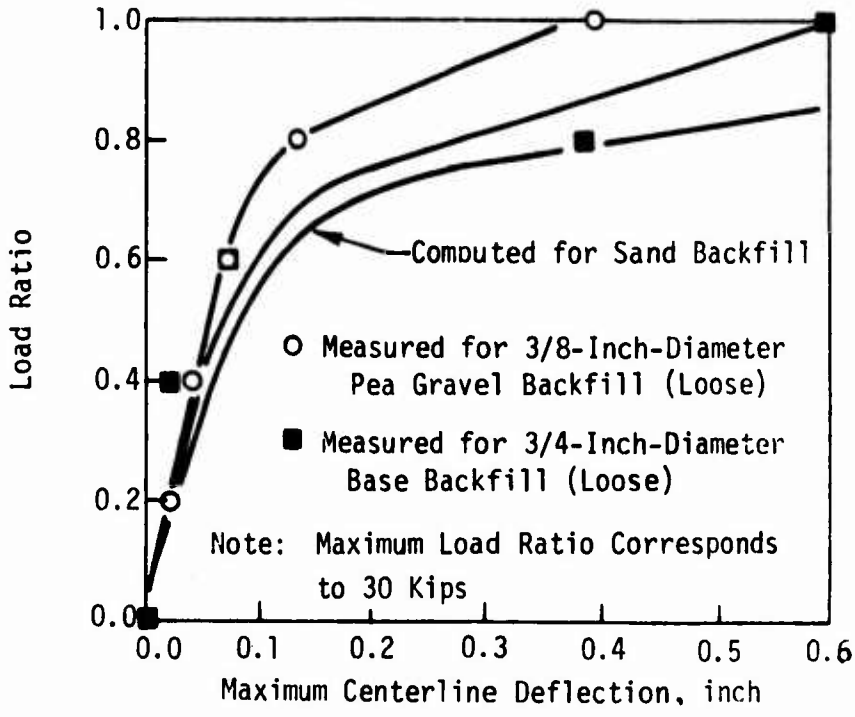

[after Forrest (Reference 8)]

Figure 20. Nonlinear Behavior of Backfill Systems

because the material properties of the compacted pushback material were unknown and the input crater cross section did not agree with cross sections presented in References 8, 10, 11, and 12. The stress profiles, along the centerline of the load (Figure 21), show a small deviation from a Boussinesq solution. This indicates that the computer model of the AM2 mat was too flexible and thus did not behave as a plate on a homogeneous soil as expected for a rigidly assembled matting. These stress profiles combined with the large computed deflections necessitated the remodeling of the element representation of the AM2 mat to obtain a greater stiffness. This was accomplished by increasing the width of the mat elements to approximately that of the AM2 section. A second analysis was performed with this stiffer model on the crushed limestone material. The effect of the stiffer model can be seen in Table 3 (first and second analyses). Vertical stress profiles from the second analysis are shown in Figure 22.

---

12. Forrest, J. B., and Lew, T. K., *A Computer Model for Predicting the Load Deflection Response of Expedient Soil Surfacings*, Technical Note N-1280, Naval Civil Engineering Laboratory, July 1973.

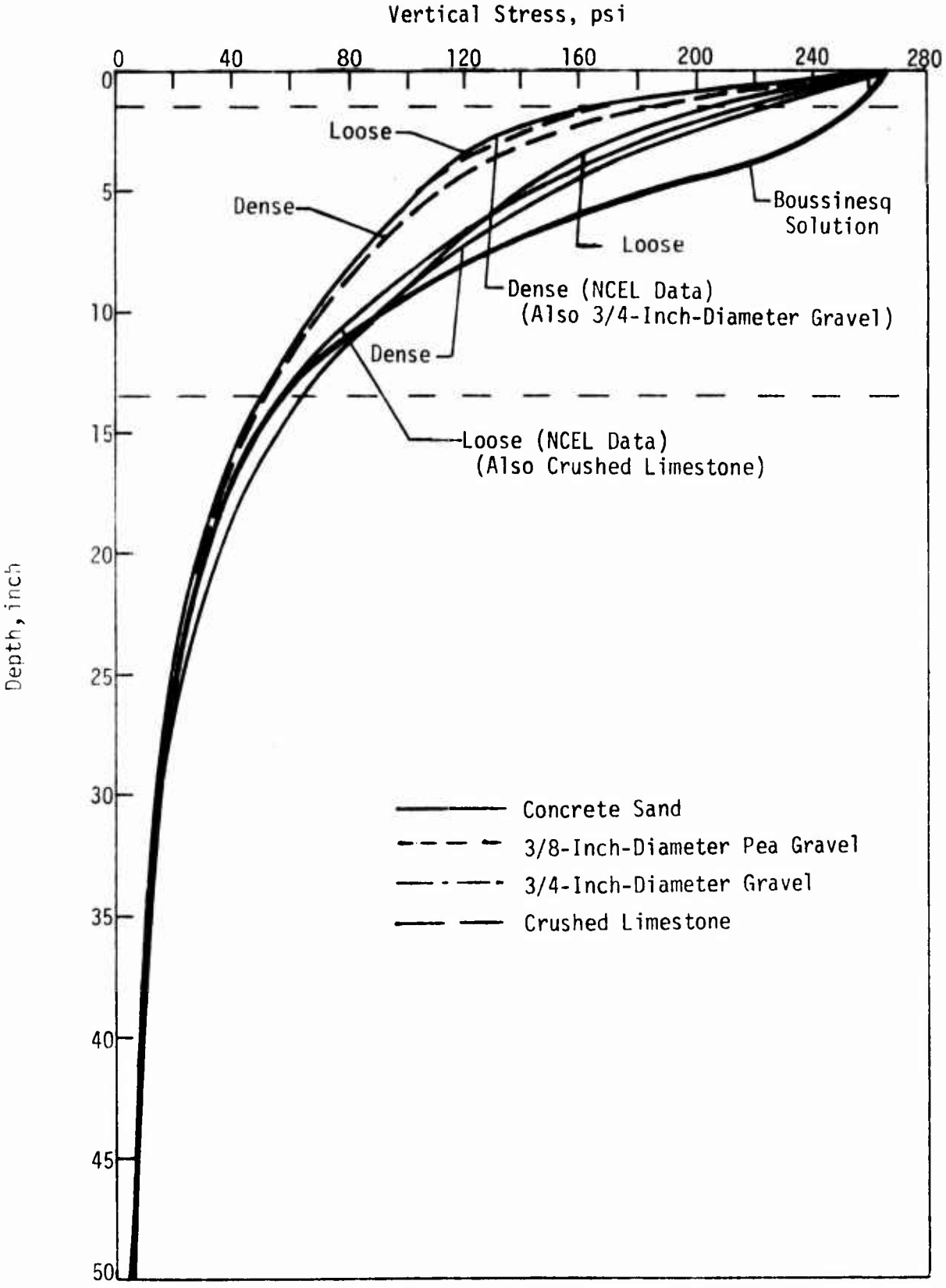

Figure 21. Vertical Stress Profiles for 12-Inch-Thick Fill Materials

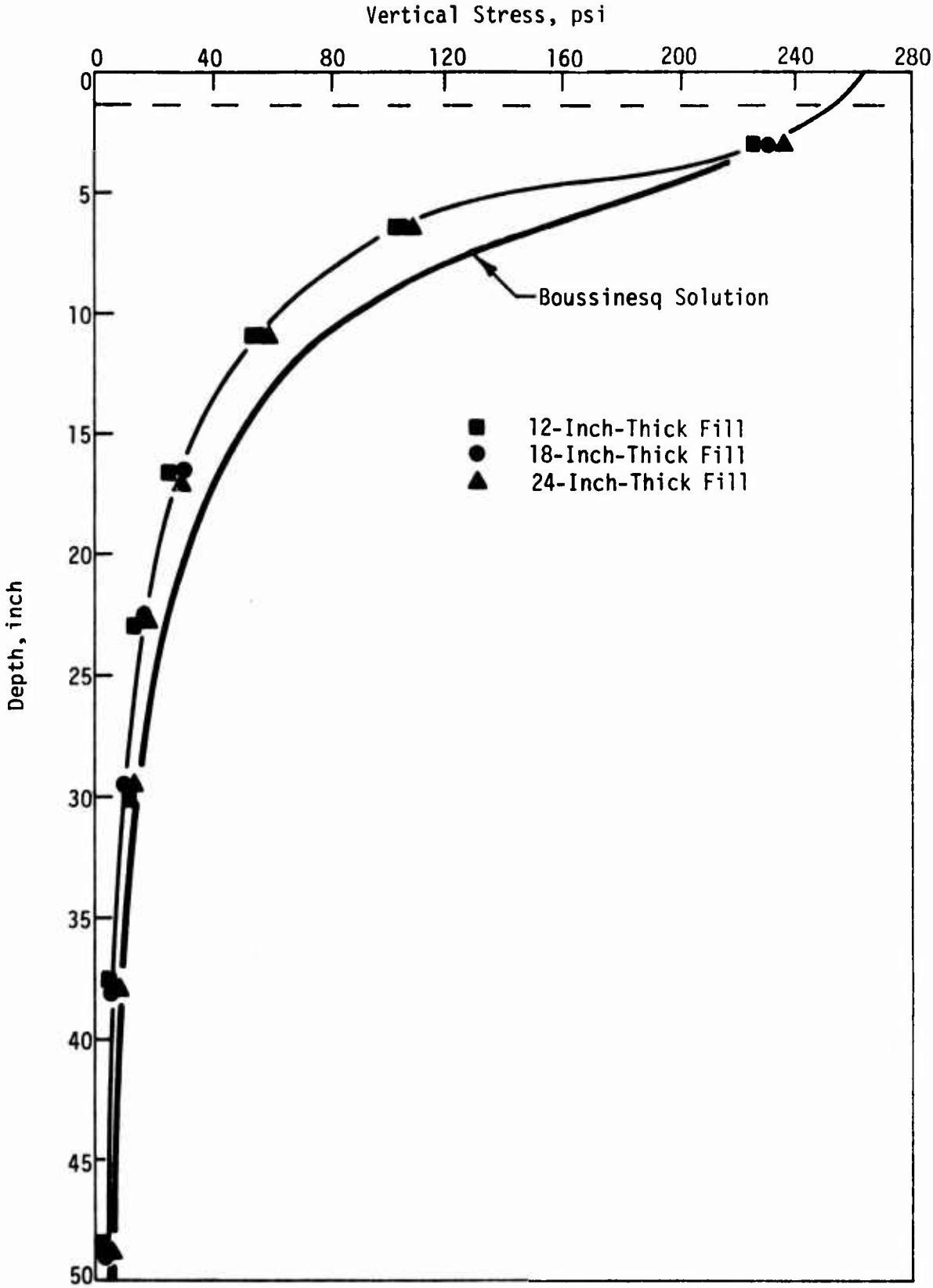

Figure 22. Vertical Stress Profiles for Crushed Limestone (Second Analysis)

Although the deflections are quite different (Table 3), the centerline vertical stresses do not appear to have varied significantly between the first and second analyses. However, this is consistent with both layered theory and the effect of increasing the size (stiffness) of the AM2 mat finite-element representation.

Crater Materials--To study the significance of the compacted pushback material on the computed deflections, the crater material properties were varied. The 3/4-inch-diameter gravel and dense sand (γ_d = 104 pcf) were used for fill materials. Figure 23 shows that the compacted pushback zone has considerable influence on the deflection, but that this influence decreases with thicker layers of fill material because the cross section changes from a layered system to a more homogeneous one. As the thickness of the fill material increases, a greater portion of the vertical stresses is contained in the fill material and the computed deflection is more representative of the fill material than of the compacted pushback material. If the thicknesses of the fill materials were increased beyond 24 inches, the curves would become more shallow and show less variation in deflection for changes in compacted pushback material properties.

Next, the assumed material properties for the compacted pushback material were used and the material properties for the fallback debris were varied to study the influence of this material on the computed deflections. These results are shown in Figure 24(a). Similar curves are shown in Figures 24(b) and (c) for the crater wall material and the undisturbed in-situ soil, respectively. However, because the properties of the compacted pushback material were assumed, the effect on the deflection of any material beneath this zone could not be accurately studied.

Linear Analysis

For the second part of the computer analysis, a range of the modulus of elasticity, E, and Poisson's ratio, μ, was selected. The bulk and shear moduli were calculated based on the elastic relationships previously given. A low, average, and high value of Poisson's ratio--0.15, 0.30, and 0.45 (Reference 4)--and nine E-values from 500 to 7000 psi were used for this analysis. This resulted in 27 runs of the BDR Code for each thickness of fill material. Only

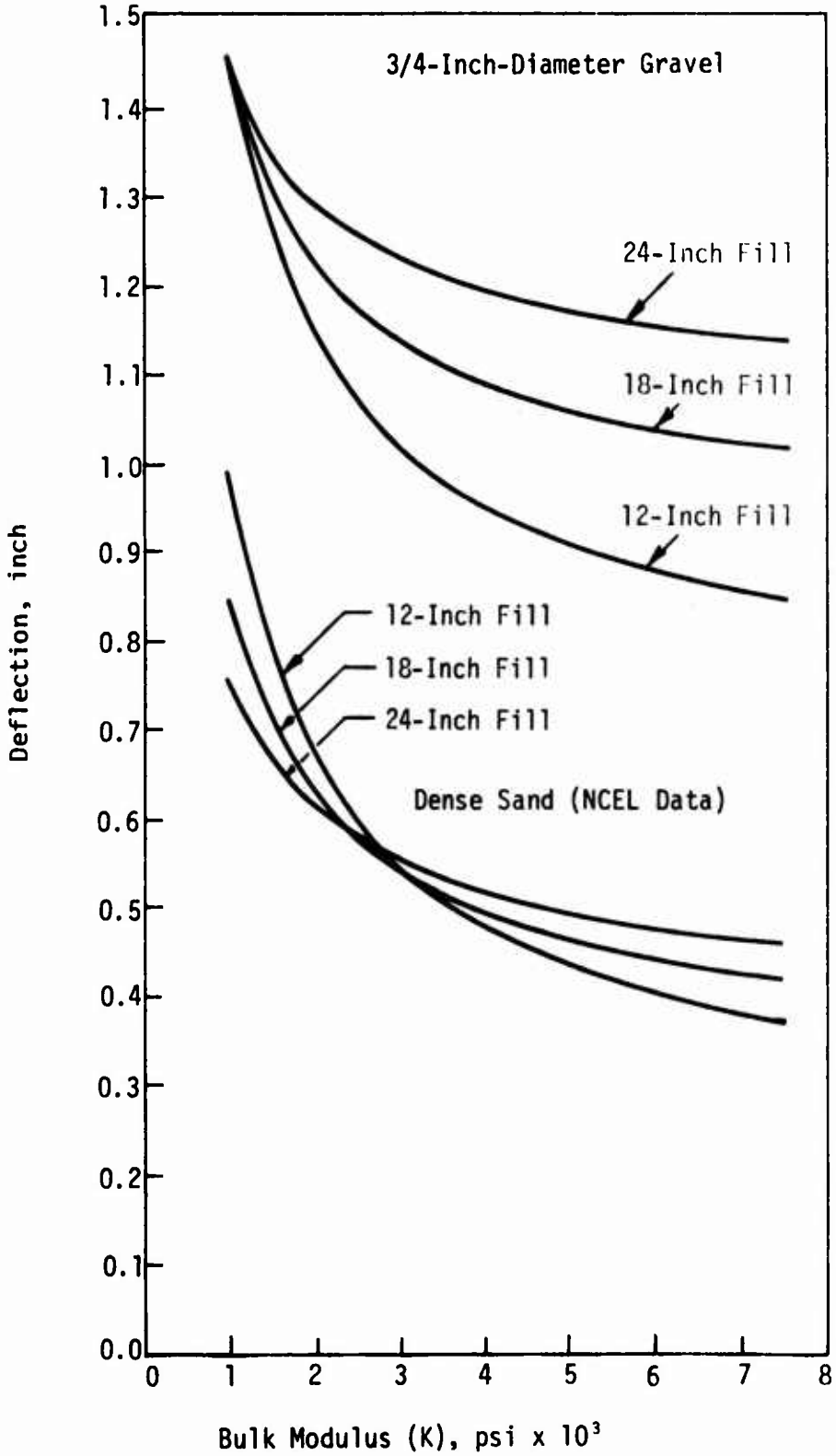

Figure 23. Effect of Compacted Pushback Material Properties on Deflection

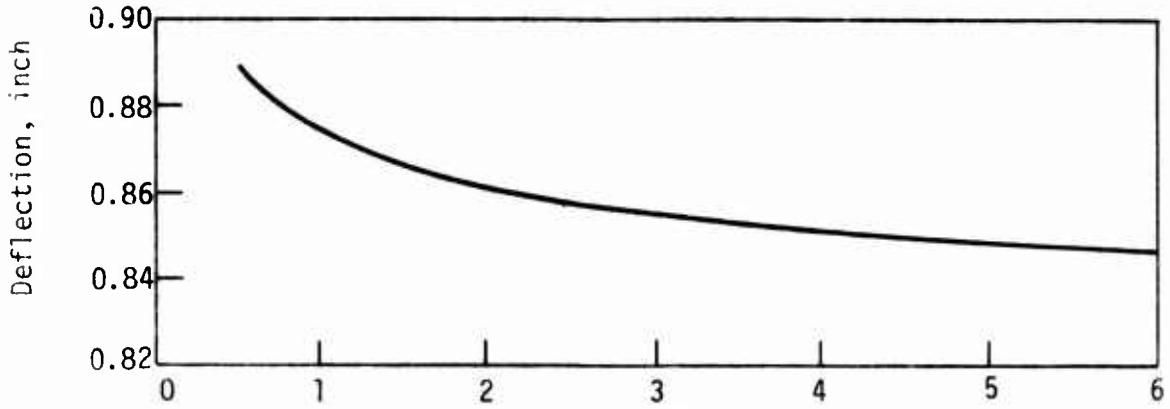

(a) Fallback Debris and Uncompacted Pushback Material

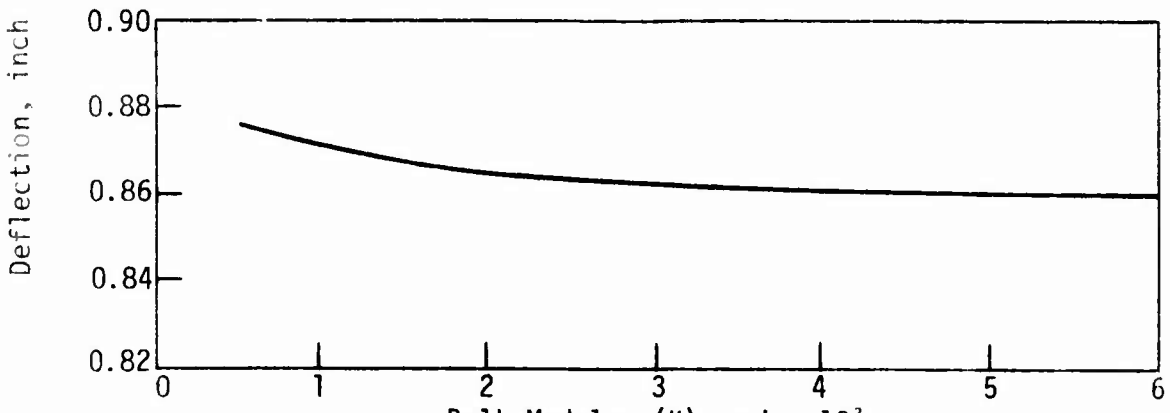

(b) Crater Wall Material

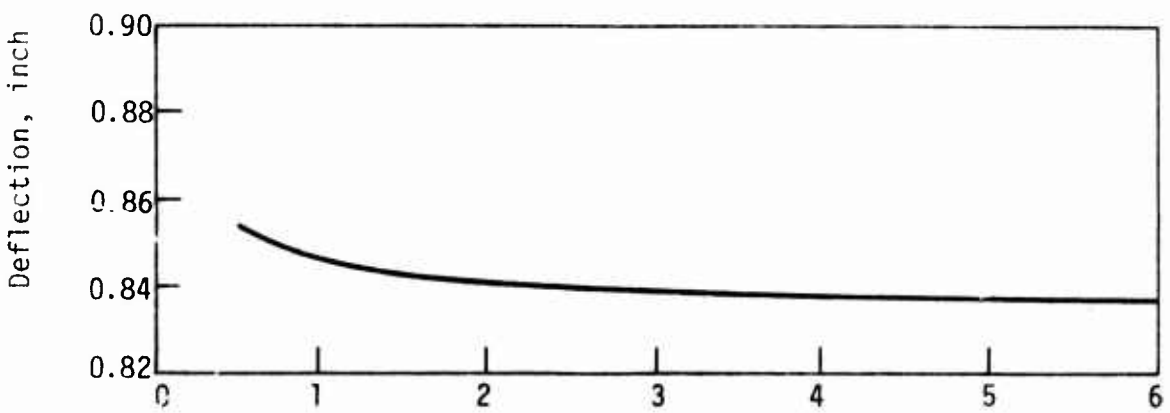

(c) Undisturbed In-Situ Soil

Figure 24. Effect of Crater Material Properties on Deflection

the properties of the fill material were changed. Figure 25 shows the results of these computer runs for the 18-inch-thick fill material. The effect of the moduli on the deflection was much greater than the effect of Poisson's ratio, especially at high E-values. The deviation of the computed deflection with the extreme values of Poisson's ratio (i.e., 0.15 and 0.45) was 20 percent at an E-value of 500 psi and less than 1 percent at an E-value of 6000 psi. This indicates that the computed deflections for a linear analysis are relatively independent of Poisson's ratio.

It was pointed out earlier that the responses of the crushed limestone and dense sand were very similar for a general state-of-stress even though the bulk and shear moduli had quite different values. The crushed limestone had a high bulk modulus and a low shear modulus and the dense sand had a lower bulk modulus but a higher shear modulus. This same effect was true for the linear analysis for varying values of Poisson's ratio; the bulk modulus decreases and the shear modulus increases when Poisson's ratio is decreased.

The effect of varying the thickness of the fill material on the deflection is shown in Figure 26. An average value of 0.30 was used for Poisson's ratio. The curves indicate a smaller deflection for the 12-inch-thick fill than for the 24-inch-thick fill. The assumed properties for the compacted pushback material are again shown to be higher than those for the fill materials. Laboratory testing of the compacted pushback material is required for a more accurate prediction of BDR crater systems.

COMPARISON OF NONLINEAR AND LINEAR DATA

The objective of this research effort was to investigate possible simplified inputs to the BDR Code that would give the same results as the nonlinear bulk and shear moduli. Linear data from conventional triaxial compression tests were used for this purpose, and data from the nonlinear and linear analyses were compared. The results, shown in Figure 27, relate the deflections computed with nonlinear input data with those computed with linear input data. The nonlinear deflection and the corresponding modulus of elasticity required by the linear analysis to yield the same deflection are shown on the upper curve. The lateral pressure for a triaxial compression test is found by entering the lower curve at this modulus value and proceeding to the appropriate

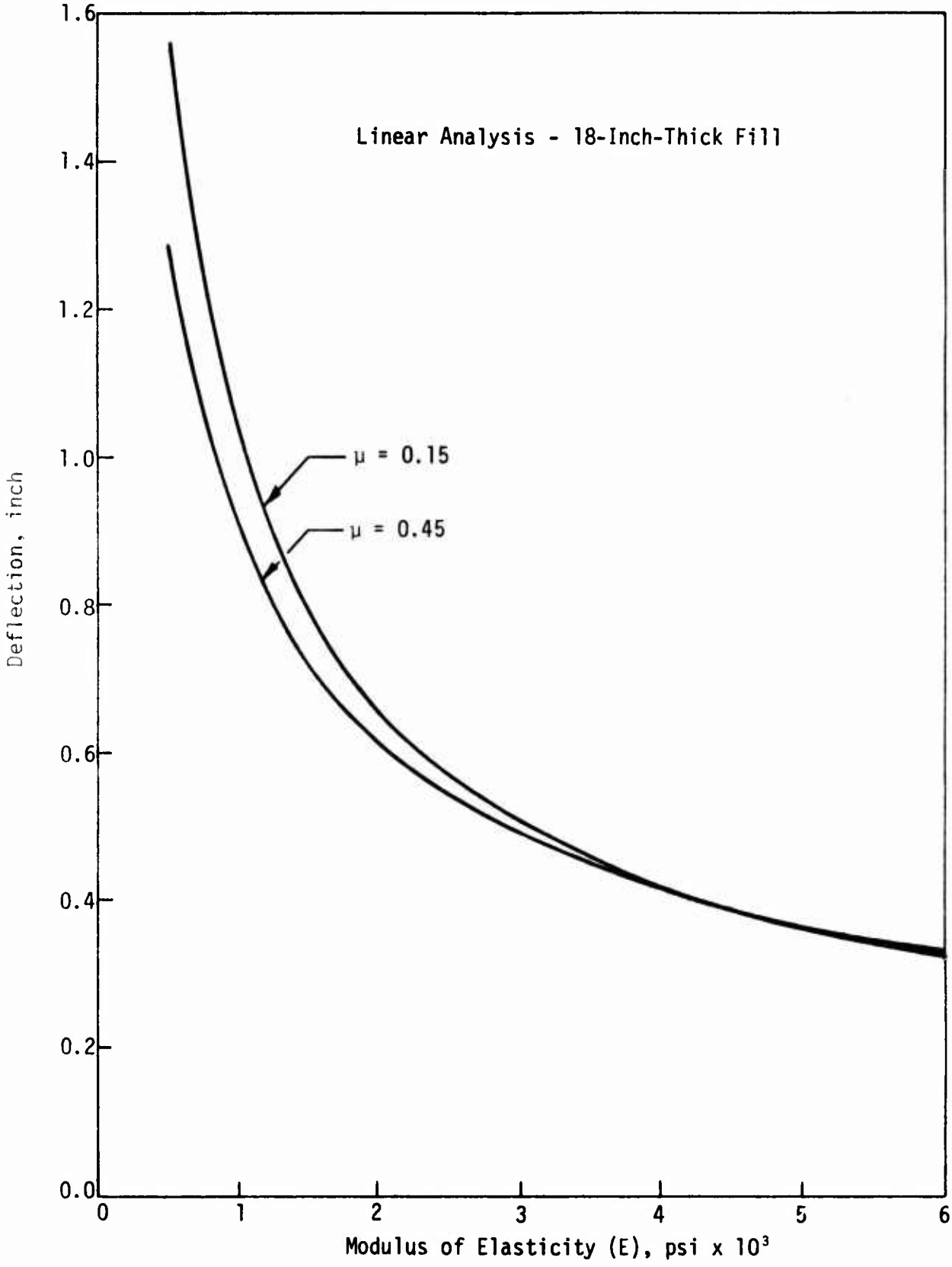

Figure 25. Effect of Poisson's Ratio on Deflection

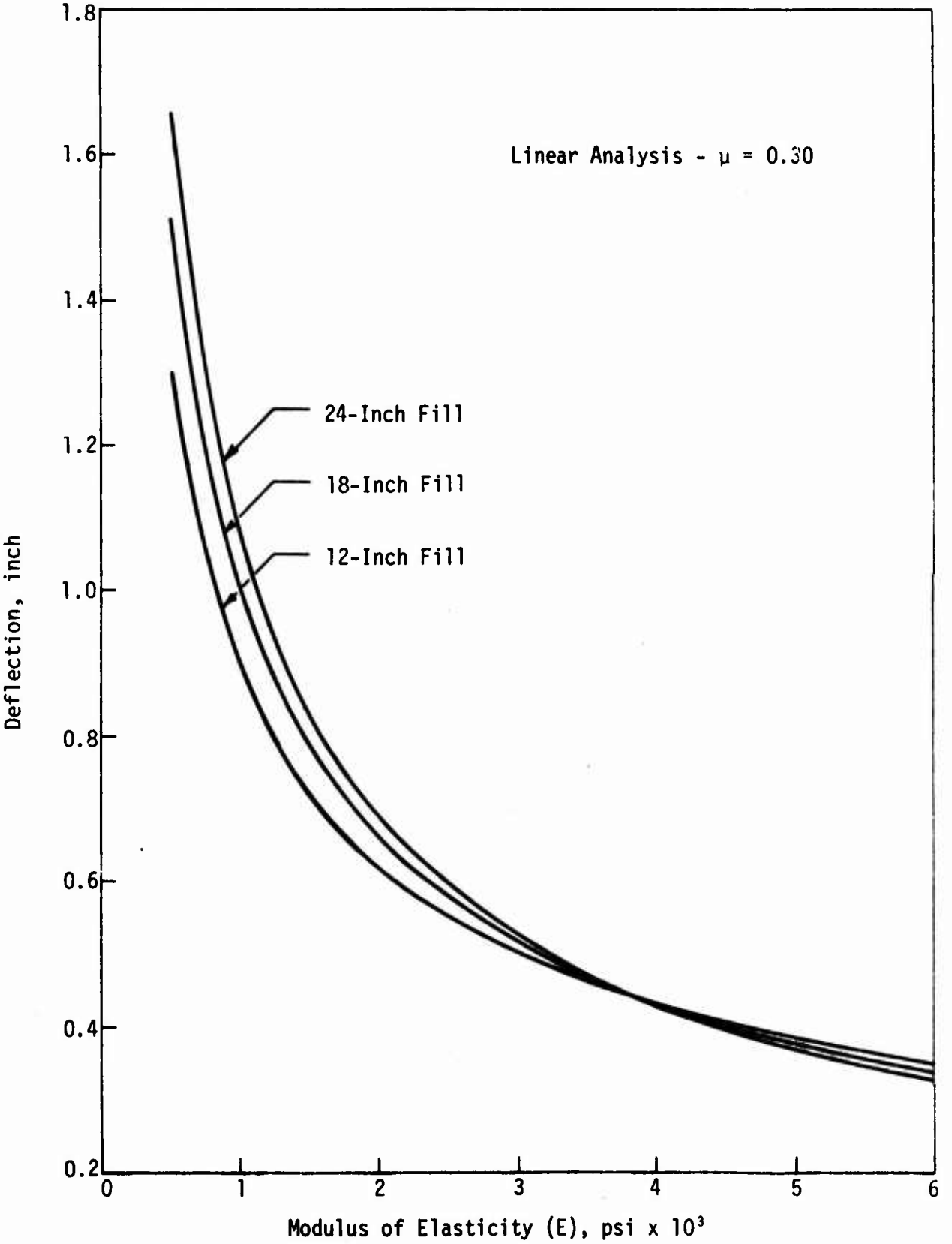

Figure 26. Effect of Fill Material Thickness on Deflection

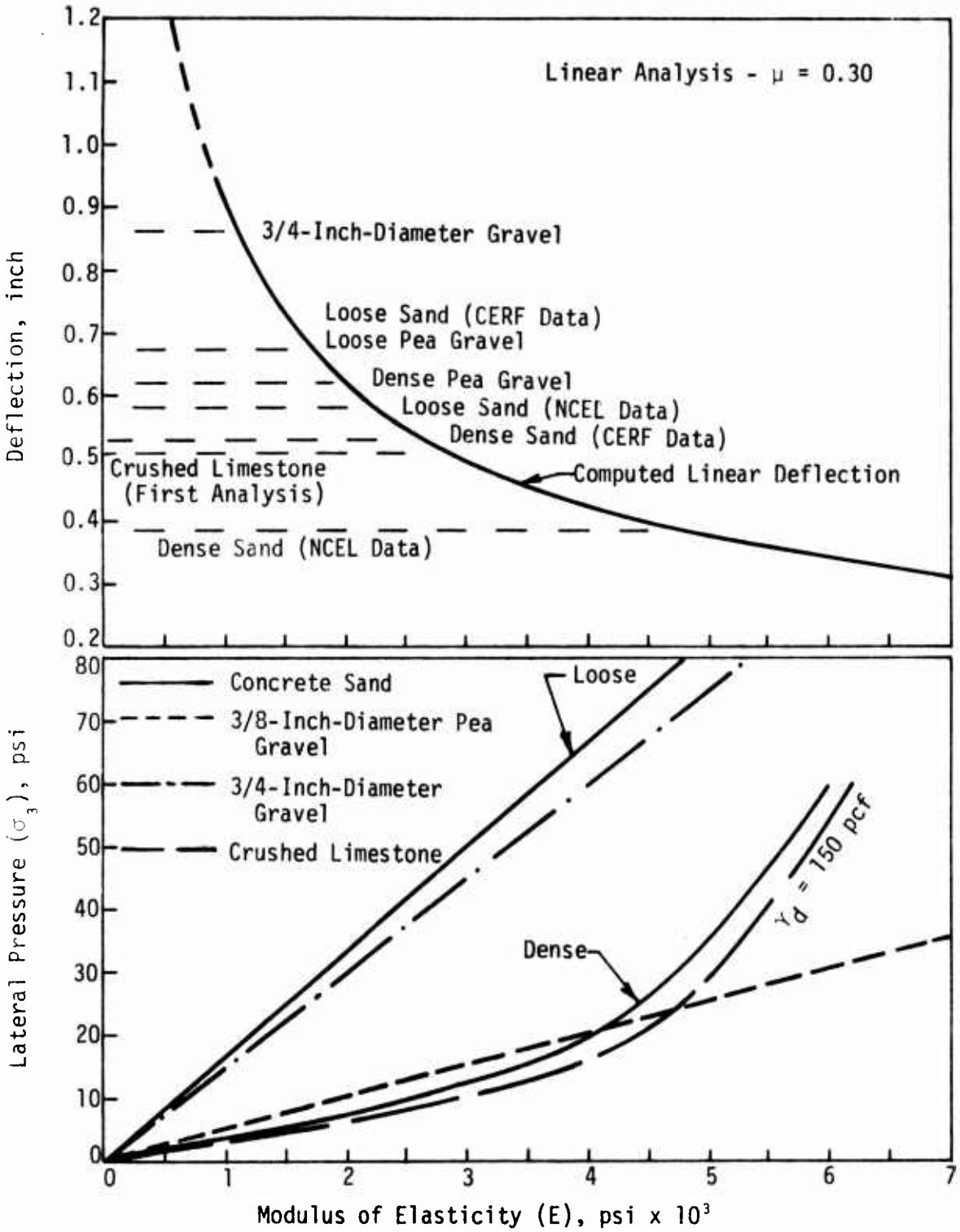

(a) 12-Inch-Thick Fill

Figure 27. Comparison of Nonlinear and Linear Analyses of Fill Materials

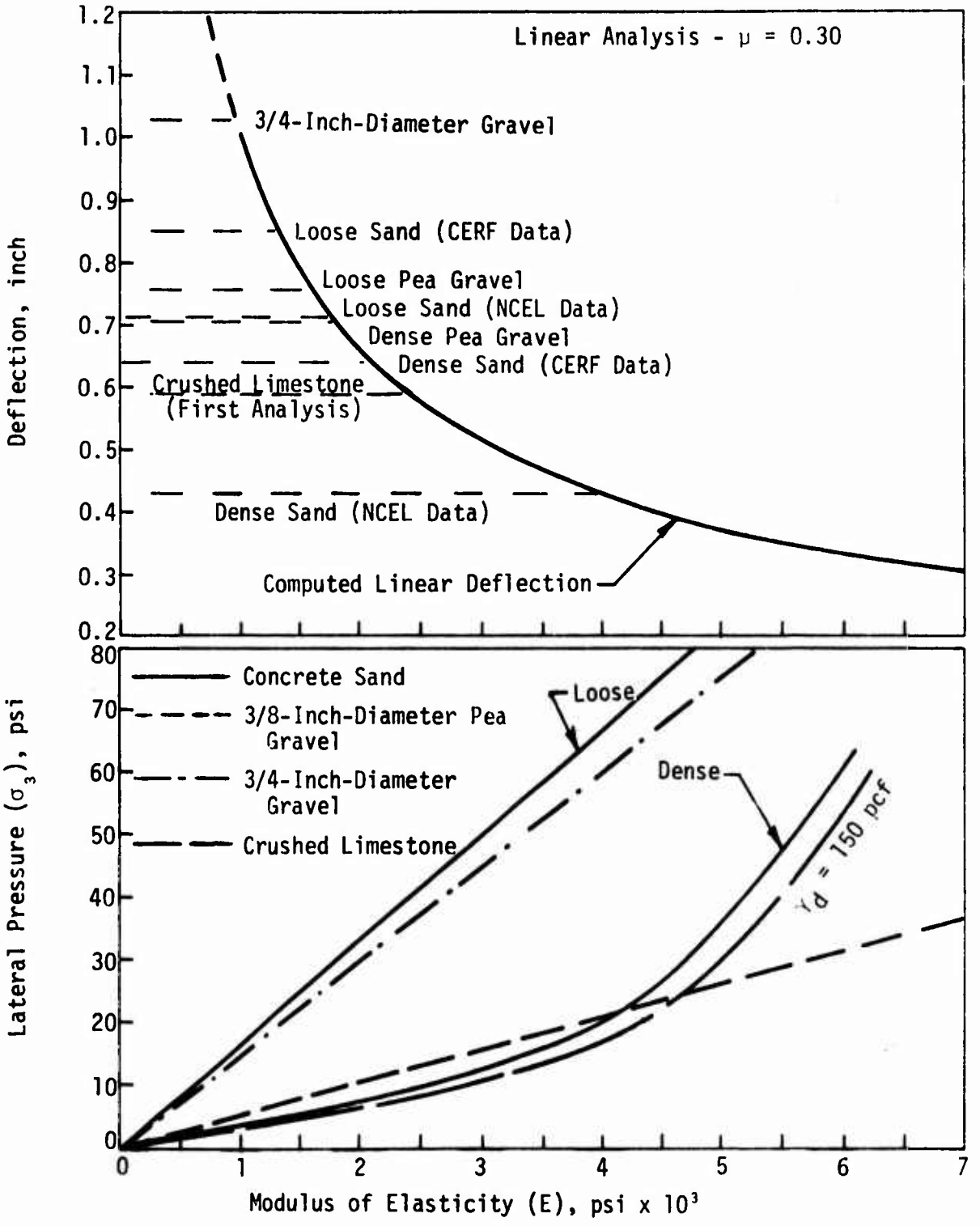

(b) 18-Inch-Thick Fill

Figure 27. Comparison of Nonlinear and Linear Analyses of Fill Materials (Continued)

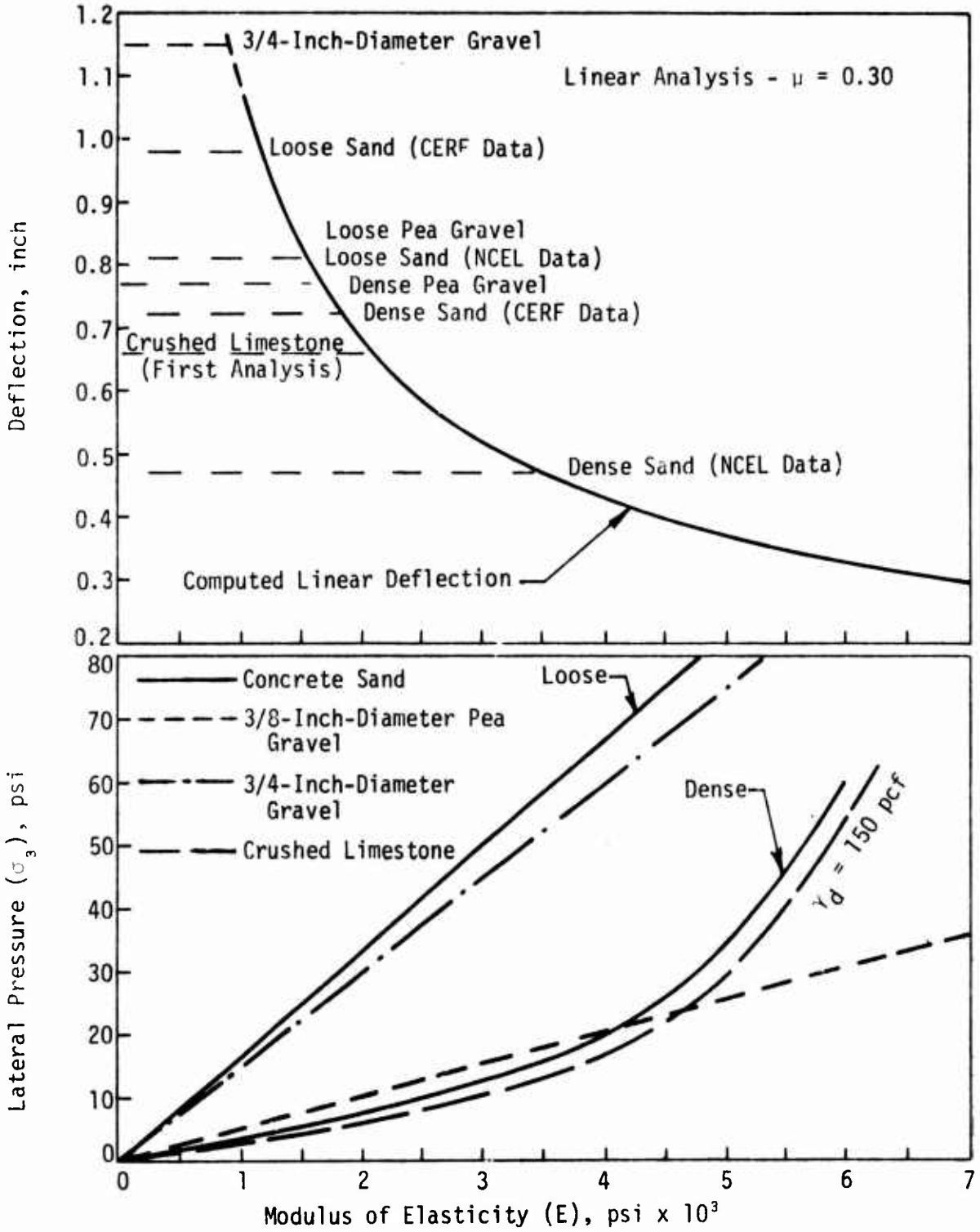

(c) 24-Inch-Thick Fill

Figure 27. Comparison of Nonlinear and Linear Analyses of Fill Materials (Concluded)

TABLE 4. SUGGESTED TRIAXIAL COMPRESSION TEST CONFINING PRESSURES

Material	Pressure (psi)
Medium/Fine Gravel	5 to 15
Dense Concrete Sand	10 to 15
Loose Concrete Sand	15 to 25
Coarse Gravel (3/8- to 3/4-inch diameter)	10 to 20
Tyndall Crushed Limestone (Well-Graded)	10 to 15

curve for the particular material. With the modulus of elasticity calculated from laboratory data, and the corresponding bulk and shear moduli as input to the BDR Code, the computed deflection will be within 20 percent of that calculated with the nonlinear bulk and shear moduli for the extreme values of Poisson's ratio (i.e., 0.15 and 0.45). The results of this data correlation are summarized in Table 4 which shows the material and corresponding lateral pressures for performing triaxial compression tests with a mean Poisson's ratio of 0.30.

Testing was performed on the crushed limestone to collect the necessary data for input to the BDR Code. A comparison of the computed deflections and the field deflections was then made to analyze the material properties and the finite-element mesh for accurate modeling. As described earlier, a redesigned mesh was used for a second analysis of the crushed limestone. This decreased the computed deflection by 30 to 50 percent (Table 3), and this decreased deflection agreed well with the measured field deflection of 0.42 inch (Reference 5). It is logical to assume that the computed deflections for the other materials would be similarly reduced and thus agree better with the field deflections (Figure 20 and References 8, 10, 11, and 12). However, making the mesh stiffer impacts on the recommendations presented in Table 4. If the user creates a crater mesh significantly different from that given in this report, the recommendations in Table 4 may not be totally valid.

SECTION VI
CONCLUSIONS AND RECOMMENDATIONS

CONCLUSIONS

Using nonlinear material properties determined from laboratory tests, the BDR Code is capable of predicting the performance of repaired crater systems. When nonlinear bulk and shear moduli determined from hydrostatic compression and constant mean normal stress tests are used, the accuracy of the results depends on the computer model of the field conditions and on the input variables of the code. Correct computer modeling and input variable selection depend greatly on the user's experience and familiarity with finite-element programs. A user's manual detailing the effect of variables on the computed output and suggesting typical values of variables for use in BDR problems would be a great help to inexperienced persons and a prerequisite if the code is to be universally accepted for BDR analysis. This report does, however, fully demonstrate that the code can be used to predict BDR crater performance.

Simplification of the nonlinear input is possible if the results from standard triaxial compression tests are used. The accuracy of the computed deflections could not be determined for all the fill materials studied because of cross-section differences between the computer cross-section input and the field cross sections. It was possible, however, to correlate computed deflections with field deflections for the crushed limestone material. This required a remodeling of the AM2 matting representation in the computer input to better agree with field conditions. The resulting finite-element mesh accurately models the BDR crater and predicts its performance. The linear-based bulk and shear moduli can be used to predict, within reasonable accuracy, a material's response to a stress condition. However, some difficulty was encountered in selecting the moduli for code input; the use of a tangent modulus can cause the predicted material response to digress from the actual field response (References 8 and 9), thereby introducing error into the predicted field response.

The Hveem Stabilometer was successfully used as a triaxial apparatus. Modifications were required to enable volume measurements to be made of the pore water

while the sample was being tested. By preparing the sample in a Proctor mold, and subsequently saturating and freezing the sample, dense samples which otherwise would not be possible can be attained for triaxial testing. The stabilometer is not meant to be a substitute for standard triaxial test equipment but an alternate for use with granular soils containing large particles which would cause difficulties with membrane puncture and sample preparation. No major problems were encountered with the laboratory techniques.

RECOMMENDATIONS

Sophisticated laboratory testing by experienced laboratory personnel is required to obtain the necessary input data for the BDR Code. In many instances, either the sophisticated laboratory equipment or the qualified personnel are not available. Both of these disadvantages can be reduced or eliminated if typical BDR materials are tested and classified according to their nonlinear response to different conditions of loading and a few soil indexes such as water content, void ratio, and gradation. Because of the lack of fill compaction, placement of backfill, and construction methods in BDR work, nonlinear material characterization is necessary. This type of data correlation has already been performed and the results have been incorporated into a finite-element, nonlinear, prismatic-solid computer program (AFPAV). AFPAV is used to compute stresses, strains, and deflections due to aircraft loading of a layered pavement system. Considerable confidence has been gained with the program; deflections have been successfully predicted within 20 percent of the measured field deflections. By including a soil constitutive model in the BDR Code, the amount of laboratory work would be greatly reduced to a few tests which could be easily and quickly performed by semi-skilled technicians.

Because of incompatibility between the PLOT2D program and the present AFWL computer software, it was impossible to obtain output from PLOT2D for the analyses performed on this project. The PLOT2D program must be modified if it is to become operational at the AFWL computer center. However, different versions of this program have successfully been used on other computer systems. It is highly recommended that the plotting routine be incorporated as an integral part of BDR analysis, both as a classroom tool and for evaluation and prediction of field response.

REFERENCES

1. Domashuk, Leonard, and Wade, Neil H., "A Study of the Bulk and Shear Moduli of Sand," *J. Soil Mech.a.Found. Div.*, ASCE, March 1969, pp. 561-581.

2. Timoshenko, S., *Theory of Elasticity*, McGraw-Hill, New York and London, 1934.

3. Desai, Chandrakant S., and Abel, John F., *Introduction to the Finite Element Method*, Van Nastrand Reinhold Co., New York, 1972.

4. Bowles, Joseph E., *Foundation Analysis and Design*, McGraw-Hill, New York, 1968.

5. Hokanson, Lawrence D., *Tyndall AFB Bomb Damage Repair Field Test, Documentation and Analysis*, AFWL-TR-74-226, Air Force Weapons Laboratory, Kirtland Air Force Base, New Mexico, October 1975.

6. Bishop, Alan W., and Henkel, D. J., *The Measurement of Soil Properties in the Triaxial Test*, Edward Arnold Ltd., London, 1957.

7. Horonjeff, Robert, and Jones, John H., *The Design of Flexible and Rigid Pavements*, University of California Press, Berkeley and Los Angeles, California, 1953.

8. Forrest, James B., and Shugar, T. A., *A Structural Evaluation of Rapid Methods of Backfilling for Bomb Damage Repair*, AFWL-TR-73-29, Air Force Weapons Laboratory, Kirtland Air Force Base, New Mexico, March 1974.

9. Crawford, John, and Forrest, James B., *A Structural Evaluation of Rapid Methods of Backfilling for Bomb Damage Repair*, AFWL-TR-74-272, Air Force Weapons Laboratory, Kirtland Air Force Base, New Mexico, August 1975.

10. Forrest, James B., and Lew, T. K., *A Computer Model for Predicting the Load Deflection Response of Expedient Soil Surfacings*, Technical Note N-1280, Naval Civil Engineering Laboratory, July 1973.

11. Frenick, W. B., *Evaluation of Washington Aluminum Company AM2 Landing Mat*, Miscellaneous Paper No. 4-753, U.S.A.E.W.E.S., Vicksburg, Miss., November 1965.

12. Grau, R. W., *Evaluation of May Two-Piece AM2 Landing Mat*, Miscellaneous Paper No. 5-68-11, U.S.A.E.W.E.S., Vicksburg, Miss., July 1968.

ABBREVIATIONS, ACRONYMS, AND SYMBOLS

BDR	Bomb Damage Repair
C_u	uniformity coefficient
E	modulus of elasticity
G	shear modulus
K	bulk modulus
p	$(\sigma_1 + \sigma_3)/2$
q	$(\sigma_1 - \sigma_3)/2$
γ	shearing strain
ε	normal strain
ε_v	volumetric strain
μ	Poisson's ratio
σ	normal stress
σ_h	hydrostatic stress
σ_m	mean normal stress
τ	shearing stress
ω	water content

INITIAL DISTRIBUTION

Hq USAF/PRE	1	RAE Farnsborough/Wpns Dept	1
Hq USAF/PREER	1	MVEE Christchruch	1
Hq USAF/PREMB	1	Martin-Marietta Corp	1
AFSC/DOB	1		
AFSC/DLXL	1		
TAC/DEE	1		
TAC/DER	1		
SAC/DEE	1		
AFLC/DEE	1		
ADC/DEE	1		
AUL/LDE	1		
AU/ED (Dir, Civ Eng)	1		
AAC/DEE	1		
AFIT, Tech Lib	1		
AFIT/DET	1		
Hq USEUCOM/J4	1		
CINCUSAFE/DEE	1		
AUL/AUL/LSE-70-239	1		
CINCPACAF/DEE	1		
CINCPACAF/DEM	1		
USAFA/DFSLB	1		
USAFA/DFCE	1		
5 AF/DEE	1		
7 AF/DEE	1		
13 AF/DEE	1		
ASD/DEE	1		
ADTC/DEE	1		
AFATL/DLJK	1		
AFATL/DLY	1		
TAWC/DEE	1		
Ballistic Rsch Lab/AMXBR	1		
WESRL	1		
WESS	1		
DDR&E (Asst Dir, Strat Wpns)	1		
AFATL/DLOSL	2		
DDC/TCA	12		
AFCEC/EM	5		
AFCEC/XRL	1		
Nav Civ Eng Corps Off Sch	1		
Naval Civ Engr Lab	2		
CRREL/EN	1		
USA/MERDC	1		
Engineers Study Group	1		
US Army Standardization Gp, UK	1		
Univ of New Mexico/Civil Engr Rsch Facility	5		

(The reverse of this page is blank)